MIT Portugal

Report for MIT Portugal Partnership (MPP2030) Research Seed Fund Program

---

Submission deadline: August 31 2023

Research title: The Effects of Working Conditions on Pollutants during Ammonia Combustion

Research Area(s): Sustainable Cities (area 4)

MIT Principal Investigator: William H. Green, Department of Chemical Engineering

Research Team and Collaborations:

- **William H. Green,** Professor, Department of Chemical Engineering, MIT. Role and contribution: overall PI.
- **Chuangchuang Cao,** Postdoc at the Green research group, MIT. Simulations.
- **Kevin A. Spiekermann,** Graduate student at the Green research group, MIT. Quantum chemical calculations.
- **Angiras Menon,** Postdoc at the Green research group, MIT. Quantum chemical calculations.
- **Valter Bruno Reis e Silva,** Senior Researcher, Polytechnic Institute of Portalegre, Portugal. Role and Contribution: PI, Experimental study of ammonia flame characteristics.
- **Alon Grinberg Dana,** Asst. Prof., Department of Chemical Engineering, Technion. Role and contribution: Kinetic model development and refinement.
- **Jose Maria Velasco,** Graduate student at the Dana research group, Technion. Role and contribution: Kinetic model development and refinement.

Executive Summary

Ammonia is a promising future energy storage medium which is carbon-free. The literature is overflowing with kinetic models to predict ammonia's reactivity. We have found severe issues with literature models, specifically inconsistent thermodynamic parameters, significant inconsistencies in some kinetic rate coefficients, and double counting of chemical species in some cases, among other issues. The goal of this work is to sort out the current state of kinetic predictions for NH_3 oxidation to advance the scientific community in understanding this system and having tools to predict its behavior and optimize the relevant applications.

We developed the first automatically generated predictive chemical kinetic model for ammonia oxidation with and without hydrogen as an additive. We performed high level electronic structure calculations to upgrade the model. A paper manuscript is underway. This final progress report mostly consists of the manuscript we are preparing, which we believe to be of high impact for the community. We also added preliminary benchmark results of the model's predictions to experimental data.

The predictive model we have generated within the MIT-PP framework enhances the current understanding of the NH_3 oxidation system, and is not merely an incremental improvement, but rather a groundbreaking progress with a new and robust approach to modeling.

1. Introduction

The Sixth IPCC Assessment Report [1] made it very clear — we need to act now to limit global temperature rise to meet the Paris agreement value of 1.5°C and avoid the irreversible impacts of climate change. [2] With increasing global greenhouse gas emissions, there is urgency to pursue all measures to develop and deploy carbon-neutral energy technologies. Therefore, one of the most significant scientific challenges our society must address during the course of the 21^{st} century is the establishment of a secure, economical, and sustainable global energy system. Since large-scale integration of intermittent renewable energies, such as solar and wind, introduces considerable uncertainty into an electric power system, an energy storage medium is required to achieve robustness. One of the promising approaches is storing energy as chemical bonds, *i.e.,* synthetic fuels. Chemical fuels have relatively high energy density, can be relatively easily transported, and the infrastructure for using fuels is essentially already in place. Alternative fuels that can be synthesized from abundant elements using excess renewable energy or off-peak conventional power are perhaps the preferred route for large-scale mid- and long-term energy storage.

Nitrogen-based alternative fuels in particular are attractive due to the abundance of molecular atmospheric nitrogen as feed stock (i.e., The Nitrogen Economy [3]). Ammonia, NH_3, is the simplest nitrogen-based fuel; it is a promising energy storage vector that has recently seen an exponential growth in interest and scientific works. [4–6] The advantages of ammonia as a fuel include a relatively high power-to-fuel-to-power (PFP) efficiency, [3] a large-scale distribution infrastructure that is already in place, [7,8] a high octane rating of 110–130, [9] and a narrow flammability range that makes it relatively safe in terms of explosion risks. Conversely, there are two primary categories of disadvantages linked to ammonia: (1.) Due to its toxicity, safety issues are a critical concern, especially in light duty vehicles. Public acceptance of an hazardous material needs to be addressed. [5] (2.) Ammonia emits a significant level of pollutants when combusted (NO_x and NH_3 residuals), and it has an overall relatively low reactivity compared with conventional fuels. [6]

The first concern mentioned above may restrict ammonia's usage to applications where professionals handle the process operate the system, such as in the case of marine vessels and power plants.[5] The health and safety concerns are manageable within existing or future protocols. The second concern of relatively low reactivity and significant nitrogenous emissions affects engine and combustor design, and requires further research and development. The relatively low reactivity of ammonia results in a low laminar burning velocity (the laminar burning velocity of a NH_3/air flame is about 20% of the respective value in a CH_4/air system[10]), a long ignition delay time, a low heat release rate, and flame instabilities. In addition, ammonia combustion generates significant amounts of NO_x, particularly via the fuel-NO pathway, and unburnt ammonia levels remain relatively high. A dual-fuel strategy, where ammonia is blended with other fuels to various extents was suggested to overcome some of these challenges. Among the possible ammonia combustion promoters are hydrogen,[11–20] syngas,[21] methane,[11,22–30] alkanes,[31,32] dimethyl ether,[33,34] alcohols,[35–37] kerosene or diesel,[38–41] coal[42,43] and biofuels.

The present theoretical work focuses on generating a detailed chemical kinetic model for the oxidation of neat NH_3 and of a NH_3/H_2 blend. This work is foundational for predicting the reactivity of ammonia with any combustion promoter. Predictive chemical kinetic models consist primarily of reaction rate coefficients and species thermodynamic parameters based on physical grounds, and are capable of numerical predictions with quantifiable uncertainties.[44] Transport parameters are also important for predicting flames, yet they are not the focus of the present work. Numerous studies have been conducted on ammonia combustion so far, and many chemical kinetic models were suggested throughout the years for NH_3 and NH_3 mixtures such as with H_2 and CH_4. These models involve detailed micro-kinetic networks of relevant elementary reaction steps, often refined using ab-initio quantum chemical computations.

More than four decades after Frederick Kaufman commented about the state of kinetic modeling and the need for critical evaluation of reaction rate data,[45,46] and although great progress has been made in the chemical kinetic modeling field since,[47–49] generating pre-

dictive chemical kinetic models still requires a significant amount of qualified individuals' time invested in an iterative, manual, error-prone, and non-standardized model generation, refinement, validation, and revision processes.[50] This results in a chaotic state that hampers advancement.[51]

Although kinetic modeling of NH_3 oxidation received significant attention lately,[37,52–71] there is still substantial disagreements on thermodynamic data and rate coefficients between different authors in this relatively small chemical system. Curran et al. has previously (2016) commented on the significant and alarming disparity of literature of thermochemical parameters, specifically of nitrogen-containing species in chemical kinetic models.[72] A similar comment about the significant discrepancies between existing literature models was also made recently by Klippenstein and Glarborg.[73] The present study shows that more than half a dozen years after Henry Curran's comment on the chaotic state of the literature, newly published literature models still have alarming disagreements and inconsistencies.

Counter-intuitively, erroneous kinetic and thermodynamic values in models may lead to compensating errors by modelers, resulting in favorable agreement between the respective model predictions and a limited set of experimental validation targets.[74] A comparative study of ammonia oxidation by Turányi et al. in 2020 concluded that there is no single kinetic model which can provide acceptable predictions for all flow reactor speciation observations.[75] Valera-Medina et al. have tested literature models and showed that none of the then-available models provide accurate predictions over a wide range of conditions.[76] Ammonia modelling indeed suffers from the "many-model" problem:[51,72,77,78] an accurate and consistent set of thermochemical and kinetic parameters is necessary. The present work attempts to advance the current state of NH_3 oxidation modelling towards this target.

The goal of the present study is to suggest a fundamental chemical kinetic model for NH_3 oxidation with and without H_2 as an additive. We begin by reviewing 18 NH_3 literature oxidation models published in the recent five years (2018–2023) and compare key parameters across these works. We then make recommendations for these parameters based on physical

grounds. Finally, we suggest an updated predictive model which could serve as a way forward in predicting the reactivity of NH_3 oxidation systems. To address the current chaotic state in modeling this system, as highlighted in Section 3.1. of the present study, we take a "data-centric" approach to model generation, where the dataset used to generate this model can be systematically enhanced to improve the performance of future models.

We hope that future NH_3 models generated or updated by the chemical kinetic modeling community will not have thermodynamic or reaction rate parameters that deviate significantly from state-of-the-art values without proper justification.

2. Methods

2.1. Chemical kinetic model generation

The model was generated using the open-source Reaction Mechanism Generator (RMG) software suite version 3.1.0.[79,80] RMG automatically explores possible intermediate species and elementary reactions for given reacting mixture and thermodynamic conditions based on reaction families and libraries using a flux-based algorithm. The generated model includes the most important species and reactions, where "importance" is defined by the user using a tolerance parameter that controls the model's size and therefore the truncation error. The procedures implemented by RMG to expand the kinetic model are extensively discussed elsewhere.[79–82] Previously, RMG has successfully generated a kinetic model for nitrogen oxidation chemistry[83] after it was extended with relevant nitrogen atom type representations and heteroatom resonance structure generation and filtration methods.[84]

The model was built based on RMG's kinetics and thermodynamic libraries and quantum chemical computations were performed as part of the present study, as described below. Thermodynamic parameters for the H/O subset were taken from Burke et al. 2012[85] and updated rate coefficients for this subset were taken from Konnov's works[86,87] which consider relevant chemically termolecular reactions showed to be important by Burke and Klippen-

stein.[88] Additional kinetic parameters were taken from a pressure-dependent computation for species relevant for hydrazine decomposition,[89] and from a carefully curated kinetics library in RMG written for nitrogen chemistry called the "primary nitrogen library".[90] The latter, discussed here for the first time, includes pertinent reactions and updated rate coefficients consisting of several major subsets related to nitrogen chemistry such as thermal NOx, prompt NOx, N_2O Pathway, NNH Pathway, NHx Pathway, N_2H_4 + N_2O_4, CH_3NO_2, thermal de-NOx, NO_2 decomposition, and HCN, among others. This library consists of about 400 reaction entries with rate coefficients from over 100 literature sources which were carefully manually-reviewed, along with rate coefficient computations reported in the present work. This RMG library represents an open maintained resource for recommended reaction rate coefficients for systems involving gas-phase nitrogen chemistry.

RMG computed phenomenological rate coefficient, $k(T, P)$, expressions from relevant high-pressure limit rate coefficients, $k(T)$'s, using an inverse Laplace transformation[91] and master equation computations via the Automated Reaction Kinetics and Network Exploration (Arkane) software.[92] Pressure-dependent reaction rate coefficient computations in this work employed the modified strong collision approximation.[93] The selected tolerance[94] for the network generation was 0.1. The model was generated for several temperature, pressure, and equivalence ratio ranges. Both neat NH_3 and a mixture of NH_3 with 10% H_2 by moles were considered, and the above equivalence ratio range relates to both systems. The input file used to generate the RMG model is provided in the Supporting Information for reproducibility and to facilitate next-generations of NH_3 chemical kinetic models using the suggested data-centric approach. Any input parameter improvements can now be reflected in updated models in a straight-forward manner. The present model is therefore herein tagged as "RMG-N 1.0". Model simulations, sensitivity analyses, and rate of production analyses were carried out using Cantera version 2.6.0.[95] Flame speed calculations were performed in Chemkin-Pro[96]

2.2. Quantum Chemical Computations

Ab-initio computations were executed automatically using the open-source Automated Rate Calculator (ARC) software,[97] an extensible codebase for automatically calculating species thermochemistry and reaction rate coefficients. Statistical mechanics processing of the electronic structure jobs executed by ARC was performed using Arkane.[92] Conformer geometry searches were carried out by ARC using a dihedral angle combination approach based on a random set of force field (MMFF94s[98]) conformers generated using RDKit.[99] Up to ten lowest energy force field conformers identified by ARC were optimized at the using the double hybrid B2PLYP functional[100] with Grimme's dispersion correction (D3)[101] coupled with Dunning's correlation consistent basis set augmented with diffuse functions, aug-cc-pVTZ.[102] level of theory. The lowest energy DFT conformer was further used. Ro-vibrational analyses were subsequently computed via ARC at the same level of theory. ARC computed a frequency scaling factor of 0.995 for this method and basis set combination using the method recommended by Truhlar.[103]

Torsional modes were automatically identified as rotatable single bonds in each species (considering relevant resonance structures[84]) and treated with continuous constrained potential energy surface optimizations with all other internal coordinates relaxed using the B2PLYP-D3/aug-cc-pVTZ level of theory at a resolution of 10^o. If a scan resulted in a lower energy structure than the original geometry, ARC took the former as the new lowest energy conformer, deleted all relevant running jobs for the species, and spawned the computations again starting from the new geometry. The 1D torsional potential energy surfaces were fitted to truncated Fourier series and used as inputs to compute energy levels and hence the partition function of the anharmonic mode using Arkane.[92]

Single-point energies were computed using the CCSD(T)-F12a method[104] combined with the correlation-consistent cc-pVTZ-F12 basis set.[105] The coupled cluster computations were performed in Molpro 2021.2.[106] Empirical systematic errors in atomization energies and enthalpies of formation associated with bond or atom types were corrected using atom energy

corrections and Petersson-type bond additivity corrections[107] implemented in Arkane[92] for the CCSD(T)-F12a/cc-pVTZ-F12 level of theory. Where possible (for 30 out of 66 species), enthalpy values at $298.15K$ were adopted from the Active Thermochemical Tables (ATcT, version 1.124),[108] replacing the computed CCSD(T)-F12a single-point energies.

All DFT calculations were performed in Gaussian.[109] All electronic structure calculations were processed by Arkane for computation of thermochemical partition function and macroscopic parameters, as well as reaction rate coefficients of interest.

Species for which geometry optimizations did not converge at several reasonable levels of theory (CBS-QB3,[110] ωB97X-D,[111] B2PLYP[100]), and after reasonable troubleshooting efforts, were manually flagged in the RMG database as forbidden to avoid adding them into the final model. For example, this procedure excluded the N_3H(T) species. An in-depth overview of non-physical species can be found elsewhere,[112] and the findings here strengthen the motivation for additional studies on this topic.

2.3. Transition state searches

Reaction transition state (TS) searches were automated using a bimolecular reaction orientation module (Fig. 1) implemented in ARC.[97] ARC's bimolecular TS search method orients two 3D structures relative to one another, with similarity to the EStokTP method by Cavallotti et al.[113] The distinguishing characteristic of ARC's approach, called the "heuristics" algorithm, is the dimensionality reduction of the problem by starting the search from the two species that contain the greatest amount of geometrical information. For the hydrogen abstraction reaction class, the two species that contain the abstracted H (R_1H and R_2H, Fig. 1) are used. This approach reduces the required degrees of freedom (DOFs) for the inter-fragment orientation problem by one relative to constructing the TS from the two reactants.

Generally, six DOFs (3 translational and 3 rotational when considering external coordinates) are required to orient two non-linear structures relative to one another in 3D space.

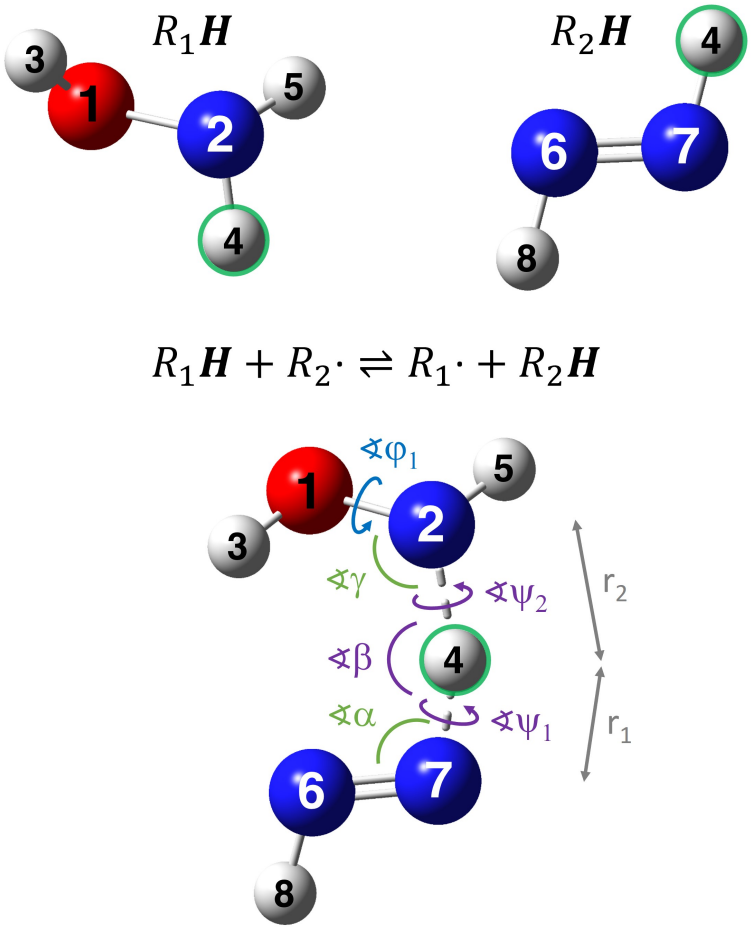

Figure 1: A 3D bimolecular reaction orientation example for $NH_2OH + \cdot NNH \rightleftharpoons \cdot NHOH + N_2H_2$. Hydrogen atom number 4 (highlighted) in each structure is superimposed when generating TS guesses.

In terms of internal coordinates, these six DOFs correspond to a bond length, two angles, and three dihedral angles, e.g., r_2, β, γ, ϕ_1, ψ_1, and ψ_2 for $R_1\cdot + R_2H$ (Fig. 1). Using the geometrical information from both R_1H and R_2H rather than, e.g., one side of the reaction such as $R_1\cdot + R_2H$, gives reasonable initial guesses for r_2, γ, and ϕ_1. The bond length values of r_1 and r_2 are stretched, e.g., by 140% each relative to their respective values in the R_1H and R_2H species, to achieve reasonable bond length guesses of the reactive zone in the TS structure. The value of β typically spans between 120^o–180^o, and any guess in this range could be used since it represents an harmonic mode. TS optimization algorithms[114] are relatively insensitive to the initial value of r_1, r_2, and β, as all three represent harmonic modes

that have a single minimum and are easily optimized. Therefor, only two challenging internal degrees of freedom, ψ_1 and ψ_2, must be determined. TS optimization cannot obtain the values for ψ_1 and ψ_2 that correspond to the global lowest energy TS structure due to the anharmonic nature of these torsional modes. These two values are therefore the only ones that are "scanned" by the algorithm to generate the TS guesses, e.g., by generating combinations of rotating these dihedral angles using a resolution of 30^o for each one.

The generated TS guesses are then optimized at an "L1" DFT level (in this case, ωB97X-D/Def2-SVP[111,115] was used). They are clustered by nearly identical internal coordinates, and representative structures from the clusters are ranked by relative electronic energy (Fig. 2). The algorithm then analyzes TS candidates in an ascending energy order and performs another saddle-point optimization and ro-vibrational analyses at an "L2" DFT level (in this case, B2PLYP-D3/aug-cc-pVTZ[100,105] was used). The algorithm terminates once one of the L2 optimized TS guesses passes reaction path energy check, normal mode displacement analysis, and intrinsic reaction coordinate[116] TS checks.

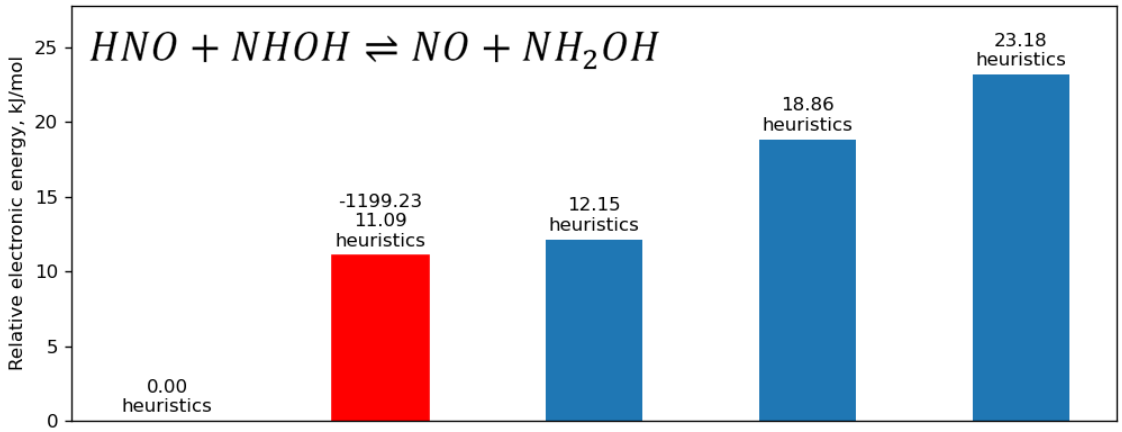

Figure 2: An electronic energy bar plot of clustered TS guesses generated by ARC for the HNO + NHOH $\rightleftharpoons$ NO + NH_2OH reaction. The lowest energy TS guess is ascribed a relative energy of 0. In this case, it did not represent a TS and failed the imaginary frequency check. The algorithm continues to the second lowest energy guess, which passes all TS checks (highlighted in red). The relative energy appears above each bar, and the imaginary frequency, if exists and a computation was attempted, appears above as well.

3. Results

3.1. Literature Parameter Review

We examined and compared 18 recent literature chemical kinetic models of NH_3 oxidation with and without additives (H_2 or hydrocarbons) published within the last five years (2018–2023).[52–69] Only the H/N and H/N/O species and reaction subsets were considered from each literature model for this comparison. I.e., we ignored all species and reactions involving carbon, where relevant, as well as the H/O subset which was already previously thoroughly studied.[85,87] Noble gases (He, Ar) were not considered in the comparison. We also do not consider in this analysis reactions involving excited species for which detailed description can be found elsewhere.[117] Within the relevant subsets the comparison study focuses on, we compared all species thermodynamic properties and discuss below reaction rate coefficients which were in significant disagreement. The purpose of this exercise is to shed light on a significant challenge confronting the broader chemical kinetics modeling community.

Code Excerpt 1: Chemkin[96] format reactions for $HONO_2$ and HNO_3 appearing in some of the literature models with respective modified Arrhenius equation parameters A ($cm^3 mol^{-1} s^{-1}$), n, and Ea (cal mol^{-1}).

```
HONO2+H=H2+NO3              5.600E+08   1.50    1.640E+04
HONO2+H=H2O+NO2             6.100E+01   3.30    6.285E+03
HONO2+H=OH+HONO             3.800E+05   2.30    6.976E+03
HONO2+OH=H2O+NO3            1.000E+10   0.00   -1.240E+03

HNO3+H=H2+NO3               5.560E+08   1.53    1.640E+04
HNO3+H=H2O+NO2              6.080E+01   3.29    6.290E+03
HNO3+H=OH+HONO              3.820E+05   2.30    6.980E+03
HNO3+OH=NO3+H2O             1.030E+10   0.00   -1.240E+03
```

All selected models attempt to capture major NH_3 oxidation pathways, and are not defined as reduced or skeletal. The number of species and reactions of the considered literature models within the relevant chemical subspace described above (H/N and H/N/O) range

between 21–26 and 170–222, respectively. Four models[57,59,60,62] did not consider the HON species, and one[64] omitted the NH_2OH species. Six of the models[54–56,58,61,65] consider both $HONO_2$ and HNO_3 species, which are suspected to be a duplicate representation of nitric acid. The two species have identical thermodynamic values in each model, so it is unlikely that one of them was meant to represent peroxynitrous acid, HOONO, which is less stable by ∼120 kJ mol^{-1} relative to nitric acid.[108,118] The duplicity is probably due to confusion when curating literature data in the process of generating one or more of these models, on which the others rely. Indeed, older studies used the different $HONO_2$ and HNO_3 notations for nitric acid.[119,120] Very similar reaction rate coefficients (Code Excerpt 1) were ascribed to reactions involving the duplicate species, appearing in the same model, supporting the assertion that the two labels correspond to the same chemical compound.

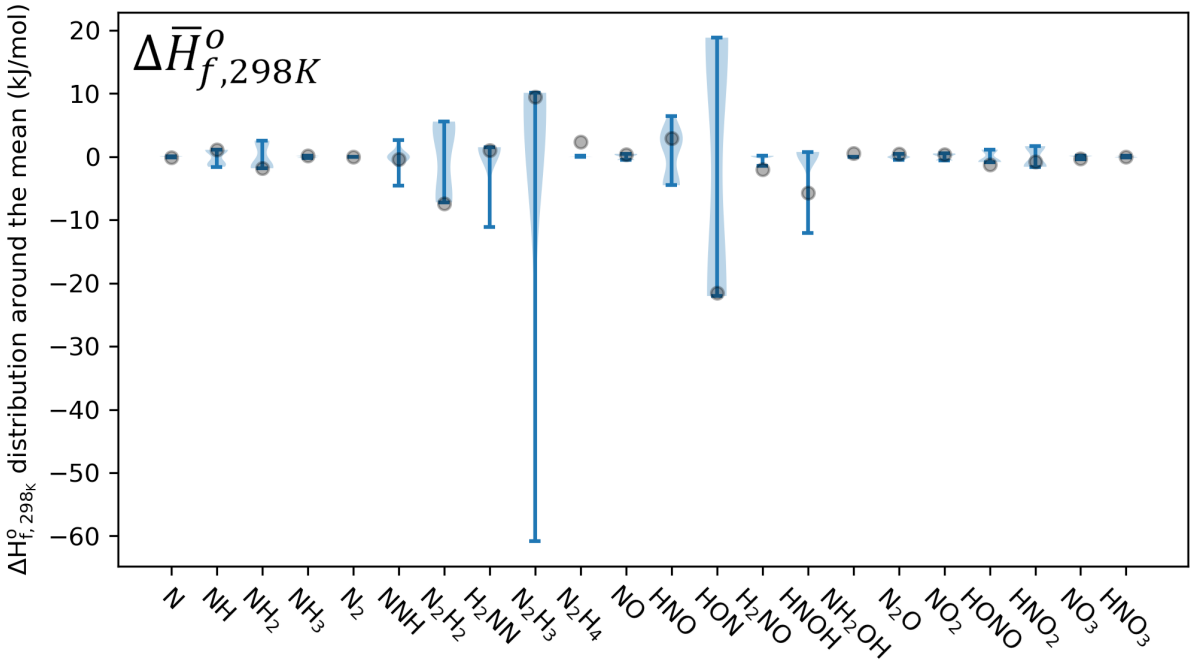

Figure 3: Distribution of standard specific enthalpy change of formation at 298 K around the mean. The bars indicate intervals surrounding the average value found in the reviewed literature models per species. The shaded "violin" areas represent the respective occurrence frequency in the examined literature models. The values for HNO_3 represent species labelled both as $HONO_2$ and HNO_3 in the examined literature models, where relevant (see text). Circles represent the deviation of the corresponding value computed in the present work relative to the average literature values.

Thermodynamic properties (ΔH_f^o, ΔS_f^o, and $\Delta G_{f,1000K}^o$) of 22 species were compared across the 18 literature models (Figs. 3–5). In these figures, larger bars represent larger value ranges that appear throughout the examined literature sources. The shaded area in each bar corresponds to the appearance frequency of each value. The circles represent the deviation of our recommended values (discussed below) from the respective average value in the considered literature sources. Other than N_2H_4, species for which a consensus in ΔH_f^o values exists between the literature sources (N, NH_3, N_2, NO, NH_2OH, N_2O, NO_2, NO_3, HNO_3) were also in agreement with our recommended values (Fig. 3). Our recommended value for ΔH_f^o of N_2H_4 is based on the ATcT,[108] and is $2.4_{kJ/mol}$ higher than the literature models value.

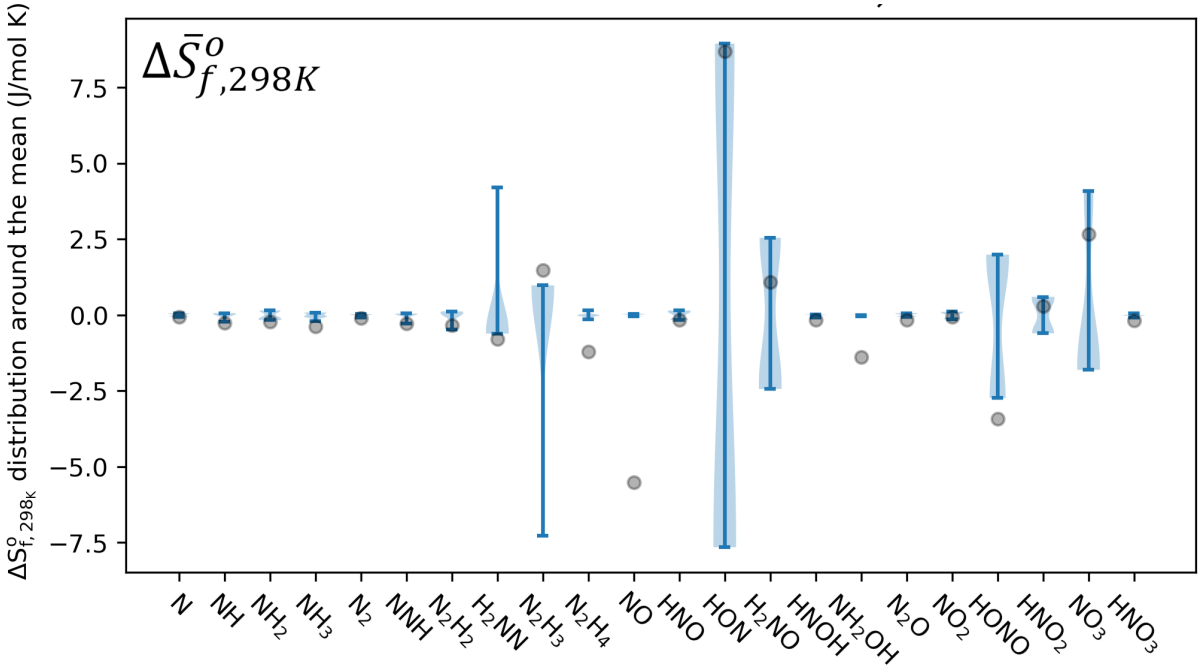

Figure 4: Distribution of standard specific entropy change of formation at 298 K around the mean. The bars indicate intervals surrounding the average value found in the reviewed literature models per species. The shaded "violin" areas represent the respective occurrence frequency in the examined literature models. Circles represent the deviation of the corresponding value computed in the present work relative to the average literature values.

Some species were found to have significant and alarming disagreements in the recent literature ΔH_f^o values. Two models[53,66] had very low ΔH_f^o values for N_2H_3, about $61_{kJ/mol}$

below the average, and about $70_{kJ/mol}$ below the ATcT value (Fig. 3). All other models used one of two values with a $5_{kJ/mol}$ difference. ΔH_f^o values for HON vary by $40_{kJ/mol}$ between the literature sources with a clear bifurcation distribution. N_2H_2 has four distinct literature values for ΔH_f^o within a range of $13_{kJ/mol}$. While the literature ΔH_f^o values for NH_2 varied by up to $4.5_{kJ/mol}$, which seems minor compared to the previously mentioned discrepancies, this variance remains troubling given the significant role this radical plays in a reactive NH_3 system.

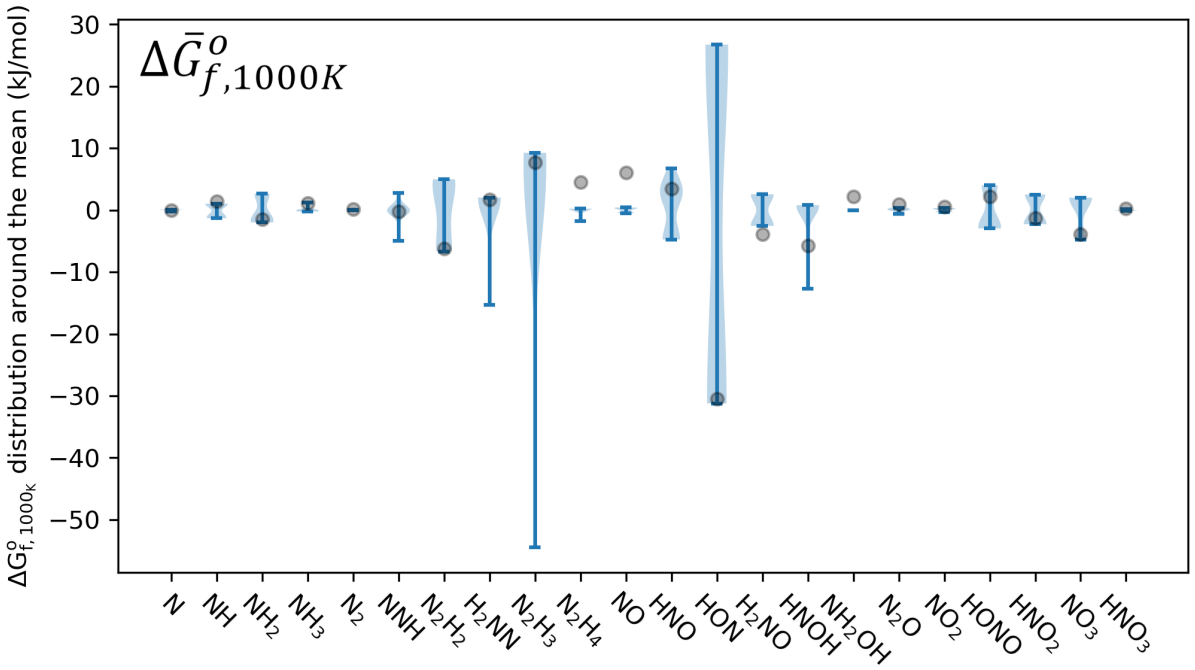

Figure 5: Distribution of standard specific Gibbs free energy change of formation at 1000 K around the mean. The bars indicate intervals surrounding the average value found in the reviewed literature models per species. The shaded "violin" areas represent the respective occurrence frequency in the examined literature models. Circles represent the deviation of the corresponding value computed in the present work relative to the average literature values.

The analysis of ΔS_f^o values (Fig. 4) reveals concerning discrepancies among recent literature references. Of particular concern, HON displays a substantial divergence of $16.5_{J/(mol\cdot K)}$, mirroring its bifurcation trend in ΔH_f^o values. Our computed ΔS_f^o values deviate from the literature's value ranges in certain instances, most notably for NO with a deviation of $5.5_{J/(mol\cdot K)}$ from the average value: about $210.7_{J/(mol\cdot K)}$ in literature models vs. our

computed value of $205.2_{J/(mol\cdot K)}$. There is indeed disagreement on the precise value, with most sources supporting $210.7_{J/(mol\cdot K)}$ [72,121] and another independent computation that supports $205.2_{J/(mol\cdot K)}$.[118] We could not settle this difference, and further analysis is welcome. There is a disagreement of $1.2_{J/(mol\cdot K)}$ in ΔS_f^o of N_2H_4 between our computation and the literature models. Our value is supported by Curran's work[72] Our ΔS_f^o value for N_2H_3 is higher than most values in the relevant literature models ($237.3_{J/(mol\cdot K)}$ vs. $236.8_{J/(mol\cdot K)}$, respectively). An even higher value of $240.4_{J/(mol\cdot K)}$ was computed by Curran et al.[72] We conclude that the current ΔS_f^o accuracy we can reach is about $3-4_{J/(mol\cdot K)}$, especially when hindered rotors are strongly coupled to an inversion mode. A multidimensional anharmonic mode treatment should be further performed for N_2H_3, N_2H_4, and NH_2OH. Our ΔS_f^o value for HONO of $248.6_{J/(mol\cdot K)}$ is lower than the range in the relevant literature models of $249.4-254.0_{J/(mol\cdot K)}$. This discrepancy is even larger in light of Curran's respective computed value of $256.4_{J/(mol\cdot K)}$. We could not settle this difference as well, and further analysis is welcome.

Gibbs free energy comparisons were made at 1000 K (Fig. 5), a practical temperature of interest for this system, and reflect discrepancies in ΔH_f^o, ΔS_f^o and Cp values. Nearly 30% of the species in the comparison have literature values that disagree by more than 10 kJ mol^{-1} in $\Delta G_{f,1000K}^o$. A similar behaviour was observed in a Gibbs free energy comparison at standard temperature (298 K) as well (not shown). Specifically, two species have their $\Delta G_{f,1000K}^o$ values scattered in a range larger than 45 kJ mol^{-1} throughout the examined literaturd models. One of these species, N_2H_3, has a deviation in $\Delta G_{f,1000K}^o$ of $\sim 4_{kJ/mol}$ between most models, while in two of the models the respective values deviate by $\sim 60_{kJ/mol}$ from the mean. The thermochemistry data of HON has a bifurcation between sources, showing a significant disagreement in $\Delta G_{f,1000K}^o$ values of $\sim 55_{kJ/mol}$. Other species that mostly show a bifurcation-type disagreement, though at a lower magnitude, are NH, NH_2, N_2H_2, HNO, H_2NO, HONO, and NO_3. The ΔG_f^o deviations of NH_2, N_2H_2, and HNO primarily stem from enthalpy inconsistencies, while their entropy values are mostly in agreement among the examined

models. The bifurcation in HON, on the other hand, is attributed to inconsistencies in both enthalpy and entropy values between literature sources.

Rate coefficient comparisons were made only between reactions defined in the same direction due to the large discrepancies found in some of the thermodynamic properties ascribed to species (Fig. 5) and the further noise this uncertain thermodynamic data will add to the reversed rates. A pressure of 100 bar was used to compare near-high-pressure limit rate coefficients of pressure-dependent reactions. Out of the 249 reactions obtained from the union of all recent 18 literature models, 43 reactions (∼17%) had rate coefficients that deviate by an order of magnitude or more. Ten reactions had rate coefficients that deviated by $\mathcal{O}(3)$ (three orders of magnitude) or more (Fig 6), among them three reactions had rate coefficients that deviated by as much as $\mathcal{O}(5)$ or more. One reaction was assigned rate coefficients that deviated between some of the models by as much as $\mathcal{O}(11)$ at 1000 K and 100 bar.

The following analysis relates to the ten reactions with rate coefficients that deviate by $\mathcal{O}(3)$ or more. One of the models[64] was missing the $HNO + HNO \rightleftharpoons N_2O + H_2O$, $N_2H_2 + H \rightleftharpoons N_2H_3$, $N_2H_3 + NH_2 \rightleftharpoons H_2NN + NH_3$, and $N_2H_2 \rightleftharpoons NNH + H$ reactions, four models[57,59,60,66] were missing the $NH_2 + NH_2 \rightleftharpoons N_2H_2 + H_2$ reaction, and 14 models (all except three[53,62,63]) were missing the $NO + HO_2 \rightleftharpoons HNO_3$ reaction.

There are five distinct rate coefficient sets for the $NH_2 + HO_2 \rightleftharpoons NH_3 + O_2$ reaction in the examined models (Fig. 6 A). We could not identify the source for the rate coefficient of this reaction from one of the models.[65] The four ultimate sources identified for the rate coefficients used for this reaction are: an experimental study by Sarkisov et al. from 1984,[122] a direct hydrogen transfer estimation for a disproportionation reaction by Dean and Bozzelli from 2000,[123] a QCISD(T) computation by Sumathi and Peyerimhoff from 1996,[124] and a W3x-L computation by Sarathy et al. from 2022.[125]

There are three distinct rate coefficient parameter sets for the $NNH + O_2 \rightleftharpoons N_2 + HO_2$ reaction in the examined models (Fig. 6 B). Their ultimate sources are: an estimation made during mechanism development by Miller and Glarborg from 1996,[126] a QRRK estimation

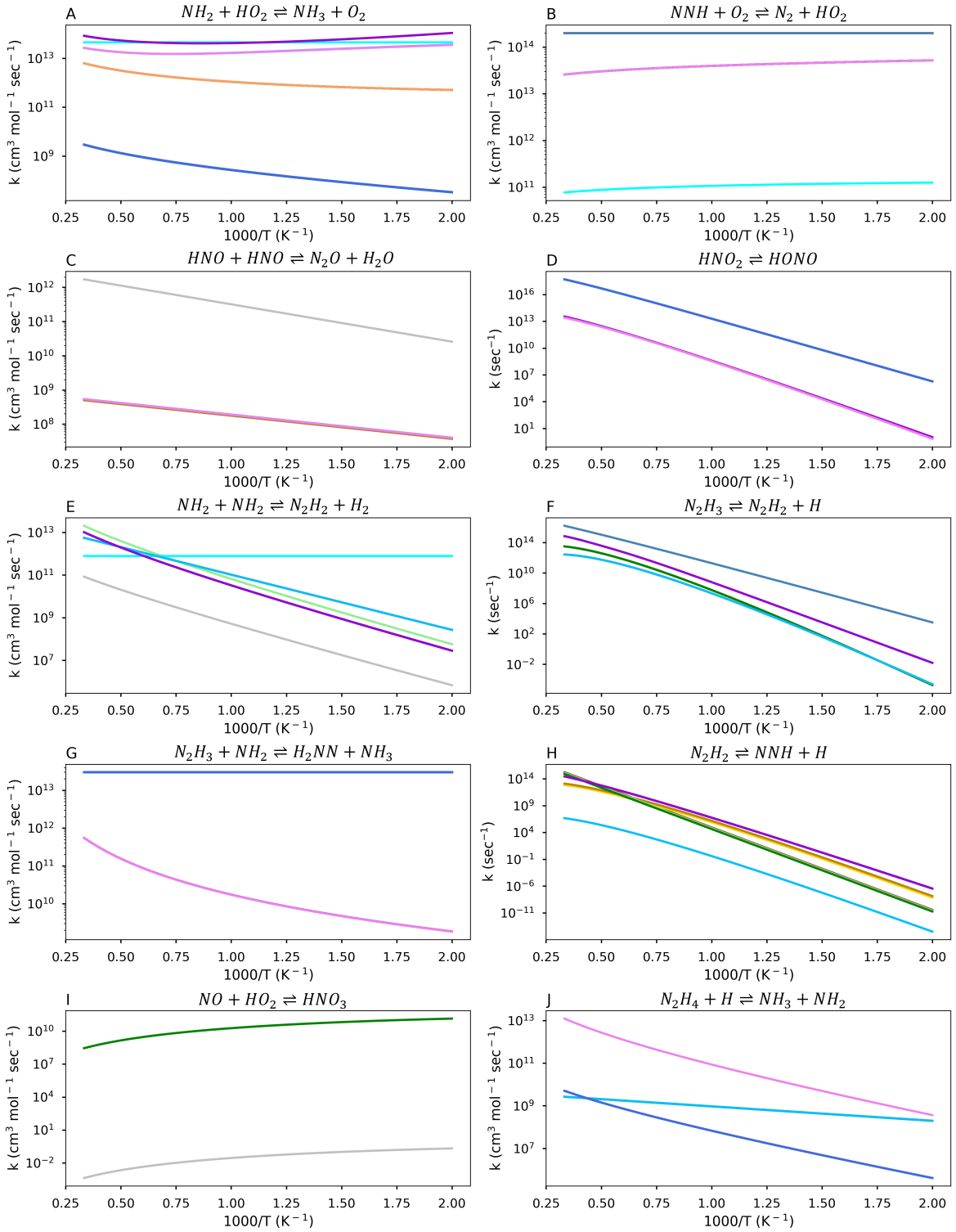

Figure 6: Rate coefficient comparison of ten reactions that deviate by $\mathcal{O}(3)$ or more among the 18 examined models. Colors represent the same models consistently throughout the comparisons. Pressure-dependent rate coefficients were evaluated at 100 bar.

by Dean and Bozzelli from 2000,[123] and a CASPT2 computation by Klippenstein et al. from 2011.[127] The value assumed by Miller and Glarborg was only a factor of 5 higher than the updated CASPT2 computation by Klippenstein et al. The Dean and Bozzelli QRRK estimation, the lowest value in this comparison, was based on the diazenyl peroxide ($\cdot$N=NOOH) intermediate species which was recently shown to be non-physical.[112]

While the updated rate coefficient for $NH_2 + HO_2 \rightleftharpoons NH_3 + O_2$ was accurately computed only recently, a trustworthy source for the rate coefficient of $NNH + O_2 \rightleftharpoons N_2 + HO_2$ has been available for more than a decade,[127] yet the later was not used by seven of the 18 examined models published in the last five years.

There are two distinct rate coefficient parameter sets for the $HNO + HNO \rightleftharpoons N_2O + H_2O$ reaction in the examined models (Fig. 6 C). All models but one used the recommended value by Tsang and Herron from 1991 from reviewing experimental observations at low temperatures (280–520 K).[128] One model[53] uses a drastically different rate coefficient with no explanation or source.

There are two distinct rate coefficient parameter sets for the $HNO_2 \rightleftharpoons HONO$ reaction in the examined models (Fig. 6 D) with two ultimate sources: a CBS-QB3 computation by Rasmussen et al. from 2008,[119] and an ANL1 level computation (based on CCSD(T)/cc-pVQZ level energies) by Chen et al. from 2019.[129] The high-pressure limit (computed at 100 bar) rate coefficients of the two sources deviate by a factor of ∼55,000 at 1000 K.

There are five distinct rate coefficient parameter sets for the $NH_2 + NH_2 \rightleftharpoons N_2H_2 + H_2$ reaction in the examined models (Fig. 6 E). We could not identify the source for the rate coefficient of this reaction from one of the models[53] (this is the same model that used a different and untraceable rate for $HNO + HNO \rightleftharpoons N_2O + H_2O$). It is also drastically different than the other literature rates (the lowest rate coefficient in Fig. 6 E). The three ultimate sources identified for this rate coefficient are: a survey by Miller and Bowman from 1989,[130] a measurement by Stothard et al. from 1995,[131] and a CCSD(T)/CBS//CCSD(T)/aug-cc-pvdz computation by Klippenstein et al.[132] One of the models[62] multiplied the Klippenstein

et al. rate coefficient for this reaction (to which the observables were sensitive) by a factor of 2 to achieve a better agreement between the model predictions and experimental results. This modification was properly reported in the respective manuscript.

There are five distinct rate coefficient parameter sets for the $N_2H_3 \rightleftharpoons N_2H_2 + H$ reaction in the examined models, one is given in the reverse direction and is not shown in the graphical comparison (Fig. 6 F). The highest rate coefficient is associated with just a single model[66] in this comparison. It was taken from Konnov 2009,[133] but could not be traced further. Updated high-level rate coefficients were computed by Truhlar et al. in 2012 for the high-pressure limit at the CCSD(T)-F12 and MRCI-Q levels,[134] and a pressure-dependent rate coefficient was computed by Diévart and Catoire in 2020 at the CCSD(T)/CBS level.[135] Besides the single intractable rate,[66] there is no significant disagreement about this rate coefficient.

There are two distinct rate coefficient parameter sets for the $N_2H_3 + NH_2 \rightleftharpoons H_2NN + NH_3$ reaction in the examined models (Fig. 6 G). The two ultimate sources are: a direct hydrogen transfer estimation for a disproportionation reaction by Dean and Bozzelli from 2000,[123] and a CCSD(T)/CBS computation by Diévart and Catoire from 2020.[135]

There are seven distinct rate coefficient parameter sets for the $N_2H_2 \rightleftharpoons NNH + H$ reaction in the examined models (Fig. 6 H). This case is somewhat concerning as there are only two ultimate sources cited for the seven rate coefficients. Another reason for concern is that the rate coefficient that does not intersect the others (Fig. 6 H) is claimed to be taken from the same source as some of the other rate coefficients, and no modification of it was reported. The two ultimate sources are: a QRRK estimation by Dean and Bozzelli from 2000[123] which gave the kinetics as two "PLOG" Arrhenius entries, each consists of Arrhenius equations for 0.1, 1.0, and 10 atmospheres, and an estimation by Mei et al. from 2019[55] based on the seminal work of Miller and Bowman from 1989[130] with an adjusted energy barrier based on computations made by Klippenstein et al.[132] The chain-branching thermal dissociation of N_2H_2, $N_2H_2 \rightleftharpoons NNH + H$, competes with its oxidation: the former

promotes the system's reactivity by $H\cdot$ production, while the latter produces less reactive $HO_2\cdot$ radicals. This chain-branching thermal dissociation reaction is critical in the overall conversion of :NH radicals into N_2,[57,59,65] and system observables such as the laminar burning velocity and laminar flow reactor speciation are sensitive to this rate coefficient.[55,60] The major disagreement in rate coefficients was caused since one of the models in this comparison mistakenly took only one of the "PLOG" rate coefficient set from the Dean and Bozzelli work. Unfortunately, another model in the present comparison inherited this partial rate coefficient "as is" in their work, citing the study which made the original data extraction mistake instead of referring to the original data source and checking for correctness and completeness.

There are two distinct rate coefficient parameter sets for the $NO + HO_2 \rightleftharpoons HNO_3$ reaction in the examined models (Fig. 6 I). As noted above, only three models in this 17 model comparison study considered this reaction. One of the sources identified is Coppens et al. from 2007.[120] The other, much lower, rate coefficient that appears in one of the compared models has identical temperature exponent and activation energy parameters as in Coppens et al. 2007, yet has an A factor lower by $\mathcal{O}(12)$. There is no mention of this reaction nor an explanation for the modified rate coefficient in the respective published work.[53] The Coppens et al. 2007 rate coefficient[120] is taken from the Konnov "Detailed Reaction Mechanism for Small Hydrocarbons Combustion" model release 0.5 from 2000,[136] yet this model is no longer available online. Hence, no ultimate justifiable source could be found for the rate coefficient of $NO + HO_2 \rightleftharpoons HNO_3$ in the compared literature models. Note that this rate coefficient was computed by M.C. Lin et al. in 1998[137] and again in 2003,[138] both at the G2M level of theory.

3.2. Recommended Parameters

3.2.1. Thermodynamic properties

We computed thermodynamic properties for 66 species relevant to the ammonia oxidation system. Table 1 lists their molecular structures. Symmetry number, number of chiral sites,

and the T1 diagnostic parameter are given in Table S1. Standard specific enthalpy change of formation and entropy change of formation at 298 K are given in Table 2. NASA polynomials[139] fitted for 298–2500 K are given in the Supporting Information in Chemkin[96] and Cantera[95] input file formats. These thermodynamic properties are also available in a maintained RMG NH3 library.[140]

Table 1: Structure of H/N and H/N/O species relevant to NH_3 oxidation

No.	Label[a]	Structure[b]	No.	Label[a]	Structure[b]
1	N	[N]	34	HNO_2	[O-][NH+]=O
2	NH(S)	[NH]	35	NH_2OO	NO[O]
3	NH(T)	[NH]	36	NHOOH	[NH]OO
4	NH_2	[NH2]	37	HONOH	O[N]O
5	NH_3	N	38	HONHO	[O-][NH+]O
6	N_2	N#N	39	NH_2OOH	NOO
7	NNH	[N]=N	40	N_2O	[N-]=[N+]=O
8	N_2H_2	N=N	41	cNNO	N1=NO1
9	N_2H_2(T)	[N][N]	42	HNNO	N=[N+][O-]
10	H_2NN(S)	[NH2+]=[N-]	43	NNHO	[O-][NH+]=[N]
11	H_2NN(T)	N[N]	44	NH_2NO	NN=O
12	N_2H_3	[NH]N	45	N_2H_3O	[O-][NH+]N
13	N_2H_4	NN	46	NH_2NOH	N[N]O
14	NH_3NH	[NH3+][NH-]	47	NH_2ONH_2	NON
15	N_3H(S)	[N-]=[N+]=N	48	N_2O_2	O=NN=O
16	N_3H_5	NNN	49	NNO_2(S)	[O-][N+](=O)[N]
17	NO	[N]=O	50	NNO_2(T)	[O-][N+](=O)[N]
18	HNO(S)	N=O	51	cNNOO	n1noo1
19	HNO(T)	[NH][O]	52	NNOO	N#[N+]O[O-]
20	HON(S)	[N-]=[OH+]	53	ON_2HO	[N-]([NH+]=O)[O]
21	HON(T)	[N]O	54	$NHNO_2$	[NH-][N+](=O)[O]
22	NH_2O	[NH2+][O-]	55	NH_2NO_2	[O-][N+](=O)N
23	NHOH	[NH]O	56	NH_2ONO	NON=O
24	NH_2OH	NO	57	HON_2HO	ONN=O
25	NH_3O	[NH3+][O-]	58	NH_2cNOO	NN1OO1
26	NO_2	[O-][N+]=O	59	cNH_2NOO	[N-]1OO[NH2+]1
27	cNOO	O1O[N]1	60	NH_2NO_2H	[O-][N+](O)N
28	NHOO(S)	[NH-][O+]=O	61	NH_2NHOO	NNO[O]
29	NHOO(T)	[NH]O[O]	62	NO_3	[O-][N+](=O)[O]
30	ONHO(T)	[O]N[O]	63	HNO_3	[O-][N+](=O)O
31	HONO	ON=O	64	N_2O_3	O=N[N+](=O)[O-]
32	HONO(T)	[O][N]O	65	$ONONO_2$	O=NO[N+](=O)[O-]
33	cNHOO	O1ON1	66	N_2O_4	[O-][N+](=O)[N+](=O)[O-]

[a] The multiplicity is explicitly given in the species label (S or T for singlet or triplet, respectively) where appropriate.

[a] Given as SMILES.[141]

Table 2: Thermodynamic properties at 298 K of H/N and H/N/O species relevant to NH_3 oxidation.Units are kJ/mol and $J/(mol \cdot K)$ for ΔH_f^o and ΔS_f^o, respectively. Computed at the CCSD(T)-F12/cc-pVTZ-F12//B2PLYP-D3/aug-cc-pVTZ level of theory.

No.	Label[a]	ΔH_f^o	ΔS_f^o	No.	Label[a]	ΔH_f^o	ΔS_f^o
1	N	472.442[b]	153.2	34	HNO_2	-43.5[b]	238.3
2	NH(S)	509.39[b]	171.7	35	NH_2OO	159.1	280.5
3	NH(T)	358.79[b]	180.9	36	NHOOH	160.8	279.6
4	NH_2	186.03[b]	194.5	37	HONOH	-0.7	274.7
5	NH_3	-45.556[b]	192.3	38	HONHO	8.4	273.3
6	N_2	0[c]	191.5	39	NH_2OOH	13.7	281.4
7	NNH	249.23[b]	224.2	40	N_2O	82.594[b]	219.8
8	N_2H_2	199.98[b]	218.0	41	cNNO	349.9[b]	241.7
9	N_2H_2(T)	377.1	234.2	42	HNNO	208.0	247.6
10	H_2NN(S)	300.46[b]	217.9	43	NNHO	314.5	250.0
11	H_2NN(T)	365.6	235.4	44	NH_2NO	76.11[b]	260.0
12	N_2H_3	224.25[b]	248.7	45	N_2H_3O	148.7	277.1
13	N_2H_4	97.57[b]	237.2	46	NH_2NOH	138.9	279.0
14	NH_3NH	281.0	239.7	47	NH_2ONH_2	132.2	271.5
15	N_3H(S)	289.4	239.1	48	N_2O_2	171.17[b]	275.8
16	N_3H_5	195.5	277.4	49	NNO_2(S)	372.5	263.9
17	NO	91.142[b]	205.2	50	NNO_2(T)	459.1	264.5
18	HNO(S)	106.97[b]	220.6	51	cNNOO	348.4	251.2
19	HNO(T)	187.7	229.2	52	NNOO	445.6	271.5
20	HON(S)	281.2	220.6	53	ON_2HO	182.3	276.0
21	HON(T)	214.98[b]	230.7	54	$NHNO_2$	236.0	284.9
22	NH_2O	64.08[b]	231.5	55	NH_2NO_2	6.1	273.2
23	NHOH	94.42[b]	233.3	56	NH_2ONO	100.1	286.2
24	NH_2OH	-43.45[b]	234.8	57	HON_2HO	52.0	295.4
25	NH_3O	60.0[b]	221.3	58	NH_2cNOO	317.4	284.9
26	NO_2	34.071[b]	240.0	59	cNH_2NOO	157.3	283.6
27	cNOO	352.6[b]	244.4	60	NH_2NO_2H	84.8	312.0
28	NHOO(S)	233.8[b]	246.6	61	NH_2NHOO	236.2	311.1
29	NHOO(T)	354.1	270.6	62	NO_3	74.14[b]	257.0
30	ONHO(T)	271.5	258.3	63	HNO_3	74.14[b]	266.6
31	HONO	-79.113[b]	248.6	64	N_2O_3	86.19[b]	301.6
32	HONO(T)	172.1	268.9	65	$ONONO_2$	40.4[b]	342.8
33	cNHOO	270.9[b]	245.9	66	N_2O_4	10.9[b]	303.9

[a] The multiplicity is explicitly given in the species label (S or T for singlet or triplet, respectively) where appropriate.

[b] Enthalpy taken from ATcT v. 1.124.[108]

[c] Exact

3.2.2. Reaction rate coefficients

We identified ten reactions for which rate coefficients varied by $\mathcal{O}(3)$ or more between literature models (Fig. 6). Table 3 lists recommended parameters for these reactions. Some reactions in this table are pressure-depended and for them only the high-pressure limit rate coefficients are given in Table 3. The pressure-dependent rate coefficient are given in the Supporting Information. Additional literature rate coefficients for $NH_2 + HO_2 \rightleftharpoons NH_3 + O_2$ (Fig. 6 A) are compared in Fig. 7. Another source for this rate computed at the CCSD(T)/aug-cc-pVTZ//M06-2X/aug-cc-pVTZ level of theory by Stagni et al. from 2020 [142] did not make it into the comparison since it was computed in the reverse direction and in our hands the reverse rate coefficient created using reasonable thermodynamic properties was unreasonably low. The Sumathi 1996 calculation, which was used by five models in the examined models, noticeably deviates from the experimental data and from the more recent computation.

Table 3: Recommended rate coefficients for the reactions in Fig. 6. Parameters are for the modified Arrhenius expression $k = AT^n exp(-Ea/(RT))$.

No.	Reaction	A[a]	n	Ea ($Jmol^{-1}$)	T range (K)	Source
1	$NH_2 + HO_2 \rightleftharpoons NH_3 + O_2$	$2.179 \cdot 10^6$	2.080	-19,920	500–1700	Ref. 125
2	$NNH + O_2 \rightleftharpoons N_2 + HO_2$	$5.6 \cdot 10^{14}$	-0.358	-544	200–2400	Ref. 127
3	$HNO + HNO \rightleftharpoons N_2O + H_2O$	$8.4 \cdot 10^8$	0	13,000	—	Ref. 128
4	$HNO_2 \rightleftharpoons HONO$[b]	$2.67 \cdot 10^{20}$	-2.80	180,400	250–2000	Ref. 129
5	$NH_2 + NH_2 \rightleftharpoons N_2H_2 + H_2$	$1.74 \cdot 10^8$	1.02	49,300	500–2500	Ref. 132
6	$N_2H_3 \rightleftharpoons N_2H_2 + H$[b]	$1.275 \cdot 10^{11}$	0.819	201,100	250–2500	Ref. 135
7	$N_2H_3 + NH_2 \rightleftharpoons H_2NN + NH_3$	$1.111 \cdot 10^1$	3.080	883.0	250–2500	Ref. 135
8	$N_2H_2 \rightleftharpoons NNH + H$	$3.8 \cdot 10^{13}$	1.2	293,000	—	Ref. 55
9	$NO + HO_2 \rightleftharpoons HNO_3$[b]	$2.85 \cdot 10^{15}$	-0.82	-174	200–2000	Ref. 138

[a] Units are s^{-1} or $cm^3mol^{-1}s^{-1}$ for first- or second-order reactions in the forward direction, respectively.
[b] Only the high pressure limit rate coefficient is given for this reaction, the complete pressure-dependent rate coefficient is given in the SI.

We computed reaction rate coefficients of 53 reactions at the CCSD(T)-F12/cc-pVTZ-F12//B2PLYP-D3/aug-cc-pVTZ level of theory. Species structures are given in Table 1.

4. Model Benchmarking

In this work, we present a comprehensive benchmarking analysis of our kinetic model by comparing its simulation results with experimental data across a diverse range of conditions. Benchmarking serves as a critical evaluation tool to assess the accuracy and reliability of the model's predictions, enabling us to validate its performance and identify areas for improvement. By conducting this thorough benchmarking analysis, we aim to establish the robustness and versatility of our kinetic model in capturing the complex behaviour of the system under investigation.

Furthermore, our benchmarking analysis covers various observables to evaluate the model's predictive capabilities comprehensively. By comparing simulation results with experimental data for different observables such as flame speed, ignition delay time and species concentrations profiles, we can assess the model's ability to capture the intricate details of the system's behaviour. This multi-observable benchmarking approach provides a more complete and rigorous assessment of the model's performance, enhancing our confidence in its predictive power.

4.1.1. Flame Speed

Flame speed is a crucial parameter when studying the behaviour of fuels and their combustion processes. Our model considers the complex network of reactions involved in the oxidation of ammonia, considering both the fuel and air components. By incorporating detailed reaction mechanisms and rate constants, we aimed to capture the intricate chemistry of ammonia combustion.

To assess the performance of our kinetic model, we compared it with experimental data obtained from a carefully controlled combustion experiment. The initial temperature was of 450 K and 1 bar of pressure with neat NH_3 as a fuel. The measurements were made at different values of equivalence ratio from 0.5 to 1.5. The equivalence ratio was defined based on the reaction $4NH_3 + 3O_2 \rightleftharpoons 2N_2 + 6H_2O$, according to the equation:

$$\phi = \frac{\left(\frac{NH_3}{O_2}\right)}{\left(\frac{NH_3}{O_2}\right)_{stoich}} = \frac{3}{4}\left(\frac{NH_3}{O_2}\right)$$

We found that our model exhibited good agreement with the experimental results, accurately predicting the flame speed and other key combustion parameters. This agreement serves as strong evidence of the reliability and general overall effectiveness of our kinetic model.

Furthermore, we also compared our model with other existing ammonia combustion models reported in the literature. The model consistently showed comparable performance against the

other models, indicating its competitive characteristic in accurately simulating the flame speed values ammonia combustion behaviour.

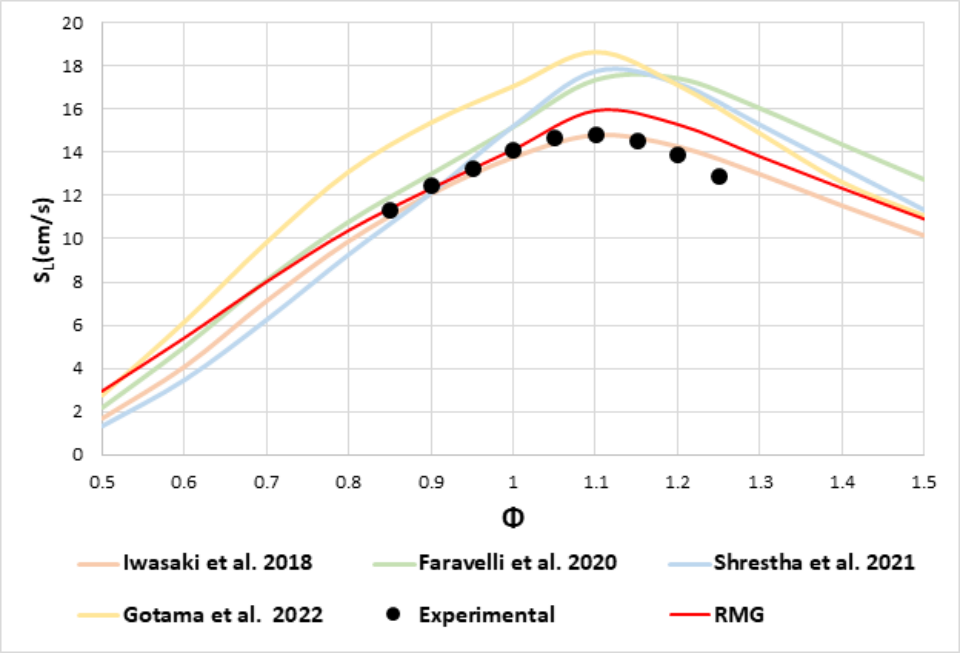

Figure 32. Flame speed comparison with T_0 of 450K and 1 bar at different Φ of our kinetic model with experimental data[106] (448K and 1 bar) and different kinetic models from the literature[62,65,70,72].

4.1.2. Ignition Delay Time

We compared our model to experimental data of Ignition Delay Time (IDT), which measures the time it takes for a specific fuel mixture to undergo oxidation and release heat under specific thermodynamic conditions of pressure and temperature. The IDT can be defined in various ways, such as the time to the maximum heat release rate (dT/dt) or the time of maximum [OH]. In our analysis, we utilized the time of maximum [OH] as the relevant IDT definition for our comparisons, among other global parameters.

The comparison was conducted at two different pressure levels, namely 20 and 40 bar, while varying the equivalence ratio at values of 0.5, 1.0, and 2.0. The results consistently demonstrate a strong resemblance to the experimental data across all cases. However, at 40 bar and an equivalence ratio of 0.5, the values exhibit slightly less agreement, although they still fall within an acceptable range.

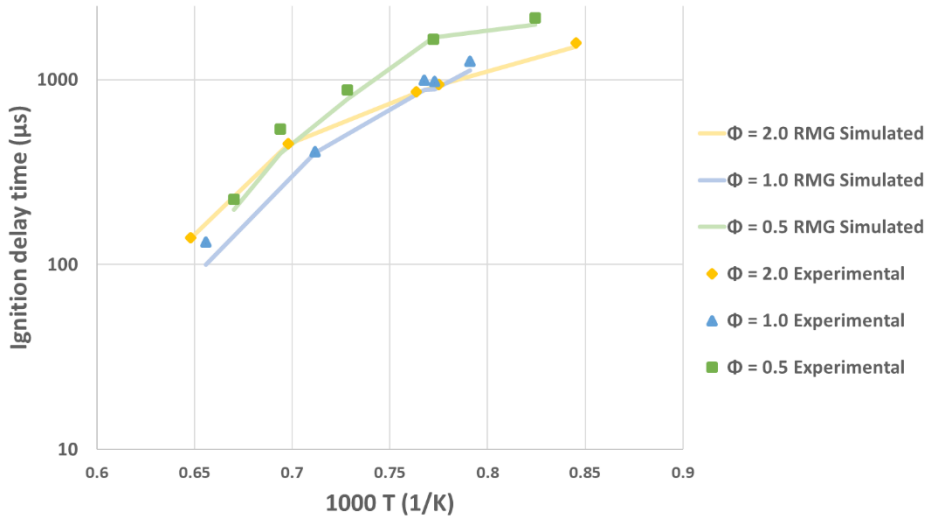

Figure 33. Ignition delay time comparison of experimental data[102] at different Φ and a pressure of 20 bar.

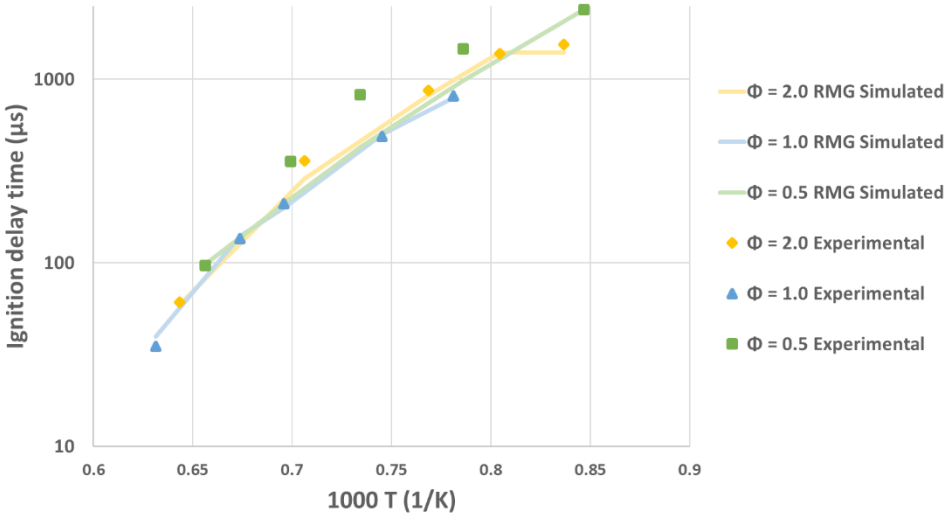

Figure 34. Ignition delay time comparison of experimental data[102] at different Φ and a pressure of 40 bar.

4.1.3. Jet stirred reactor I

This simulation was performed following the conditions established in Stagni et al. 2020[65]. The authors carried out experiments for NH_3 oxidation in a Jet Stirred Reactor (JSR) with helium as bath gas, by oxidizing 500 ppm of ammonia with 2% and 4% oxygen, respectively. The corresponding Φ values were consequently very low, 0.0188 and 0.0093,

respectively. Results are shown in Figures 35 - 38 for NH_3 and NO mole fractions. NO_2 was also measured but was not experimentally detected in this experimental series in agreement with the simulations predicting maximum values of ~1.4 ppm (Shown in Figure 1 A1.3 and Figure 2 A1.3 in annex 1).

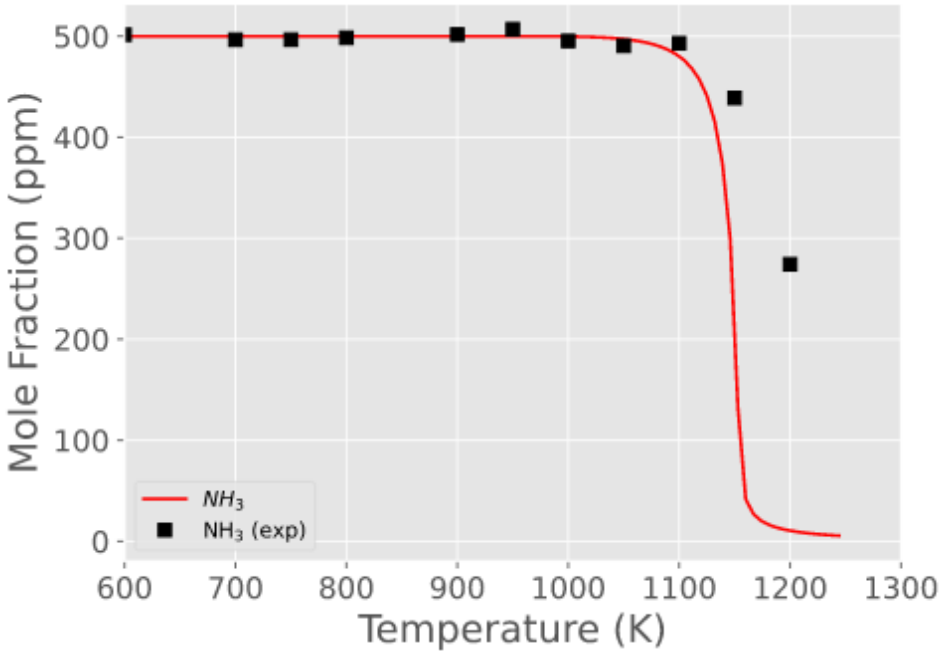

Figure 35. Oxidation of 500 ppm of NH_3 in a JSR. Experimental[65] and modelling results for NH_3 at Φ = 0.0188, P =1.06 bar, τ = 1.5 s with 2% O_2.

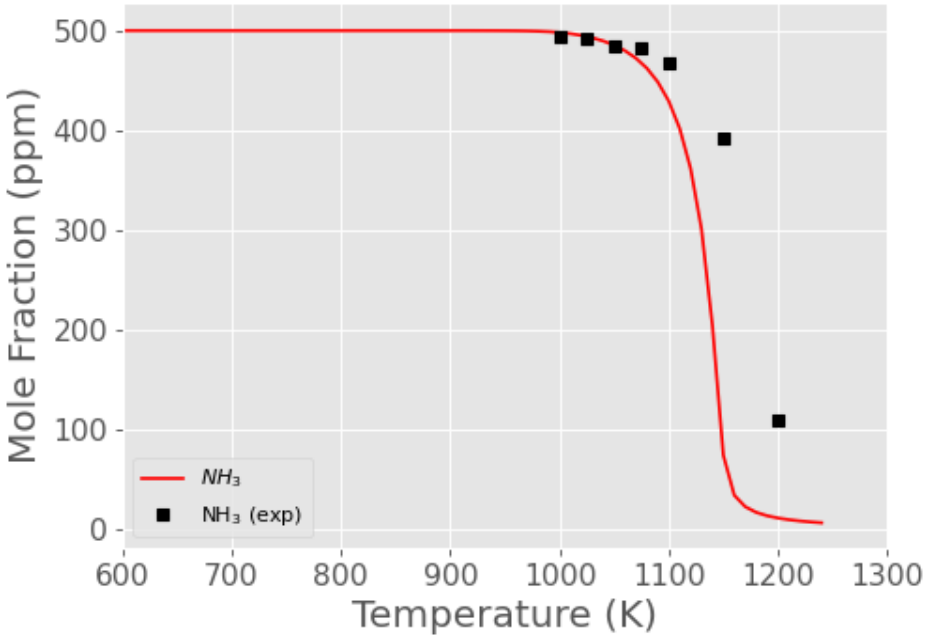

Figure 36. Oxidation of 500 ppm of NH_3 in a JSR. Experimental[65] and modelling results for NH_3 at Φ = 0.0093, P =1.06 bar, τ = 1.5 s with 4% O_2.

We can observe that, considering the high oxygen concentration present, the reaction starts at relatively high temperatures, i.e., at ~1025K and ~1000K for 2% and 4% oxygen, respectively. In both cases, the consumption of NH_3 occurs relatively rapidly with increasing temperature, being halved after just a ~125 K increase from the reactivity onset for the 4% case and after a ~100 K increase from the start of consumption for the 2% case, respectively. The kinetic model is able to predict the experimental data behaviour, although at temperatures higher than 1200 K, it predicts slightly less concentration (mole fraction ppm) than what's presented in the experimental data.

A satisfactory agreement can also be seen for NO. However, the experimental data shows an earlier formation of NO with 4% oxygen (~1 ppm at T = 900 K, where NH_3 conversion is close to zero) and our model starts NO production at ~970 K. The shape of NO concentration profile is well predicted in the case of 2% oxygen, in particular at the temperature range of 1000 K – 1150 K, although our simulations increase NO concentrations more quickly and steeply than what the experimental data marks at high temperatures ~1200 K. In the case of 4% oxygen, the trend is represented correctly, but the shape is not as accurate. The experimental data presents the NO profile having a double inflection point, and this is not seen in our simulation, we predict a steady increase of the concentration, which we consider to be a more physically plausible behaviour.

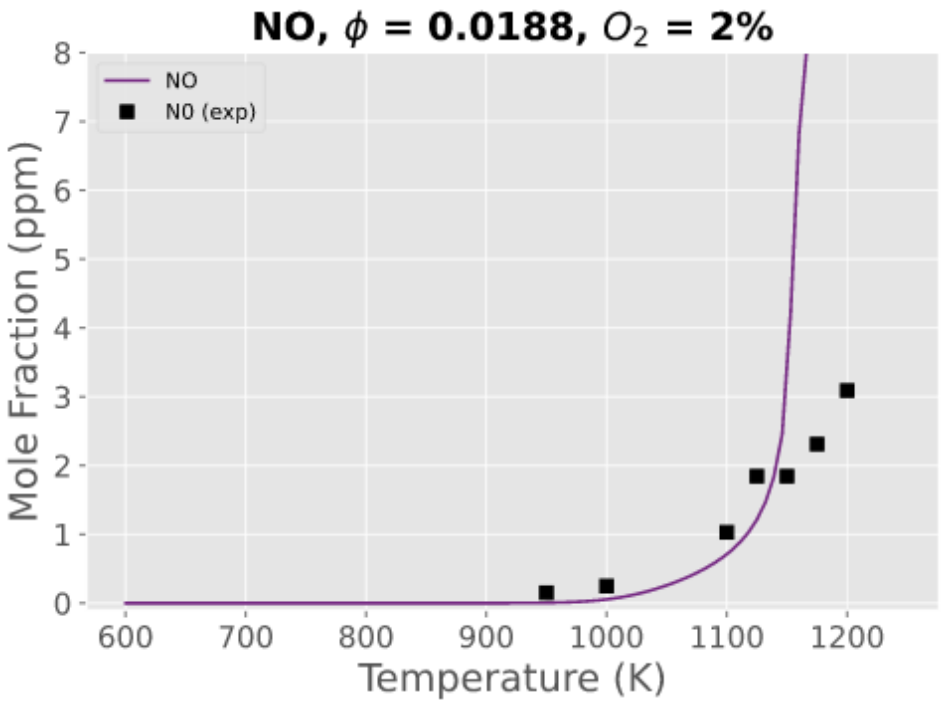

Figure 37. Oxidation of 500 ppm of NH_3 in a JSR. Experimental[65] and modelling results for NO at Φ = 0.0188, P =1.06 bar, τ = 1.5 s with 2% O_2.

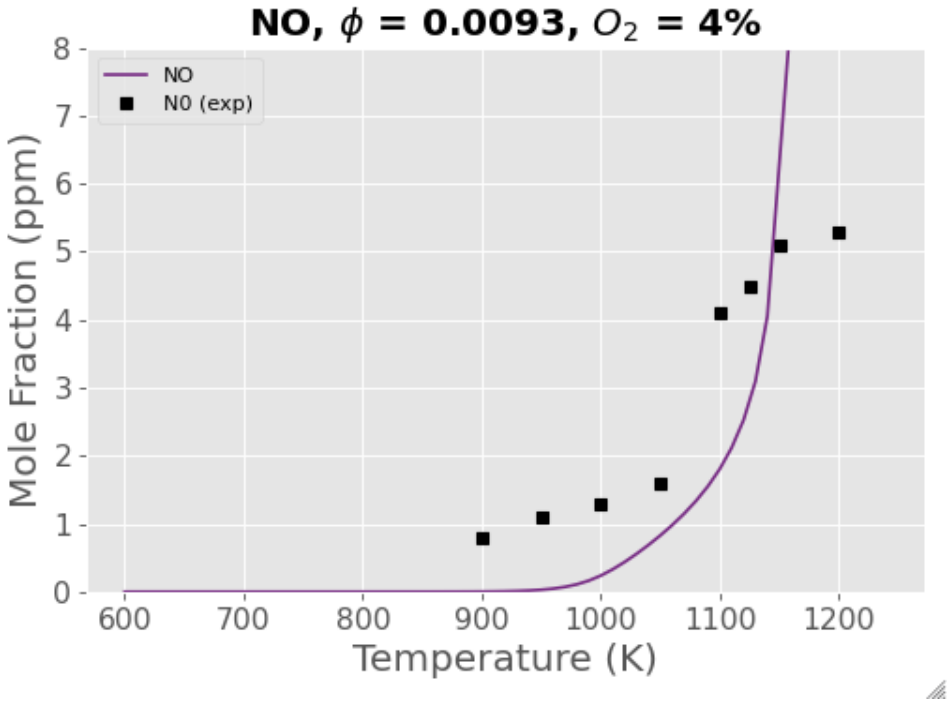

Figure 38. Oxidation of 500 ppm of NH_3 in a JSR. Experimental[65] and modelling results for NO at Φ = 0.0093, P =1.06 bar, τ = 1.5 s with 4% O_2.

4.1.4. Plug Flow Reactor

Ammonia oxidation was simulated above 1300 K compared with experiments reported in Stagni et al. 2020[65]. This experimental data was obtained by injecting 1000 ppm NH_3 with 2000 ppm O2 (Φ = 0.375) meaning its lean conditions. Figures 39 - 44 show a comparison between the measured and simulated mole fractions for the major species, NH_3, O_2, N_2, H_2, H_2O and NO.

Ammonia conversion initiates at ~1400 K, and is complete above 1500 K. In this temperature interval, H_2 is formed as an intermediate product, with an observed peak of about 50 ppm. N_2 and NO are the major nitrogenated products, with the NO yield progressively increasing with temperature.

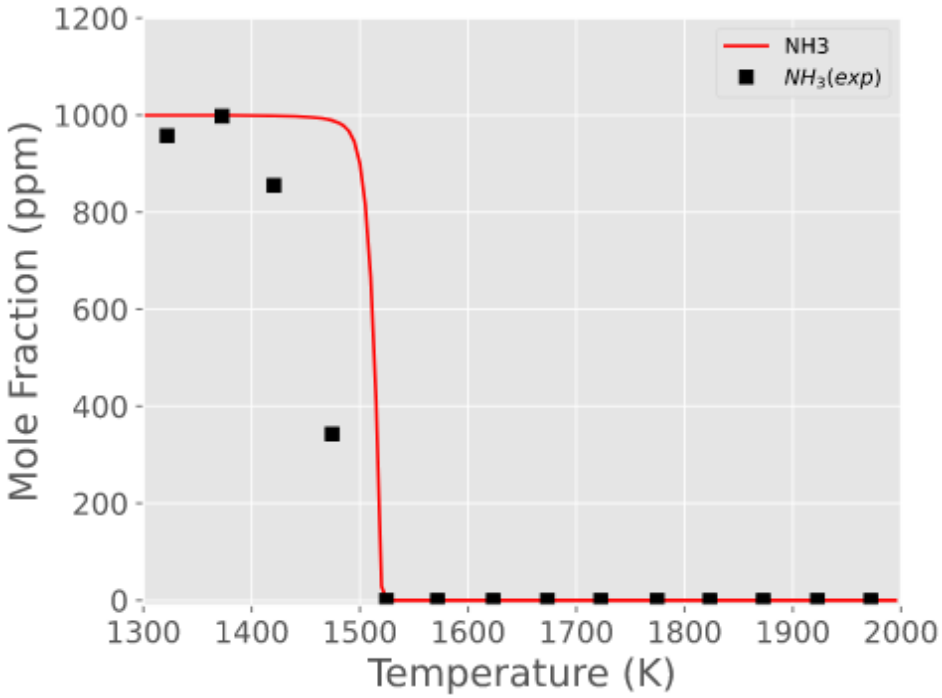

Figure 39. Oxidation of 1000 ppm NH_3 with 2000 ppm O_2 in a PFR. Experimental[65] data and modelling results comparison of NH_3 concentration profile. P = 1.27 bar, Φ = 0.375.

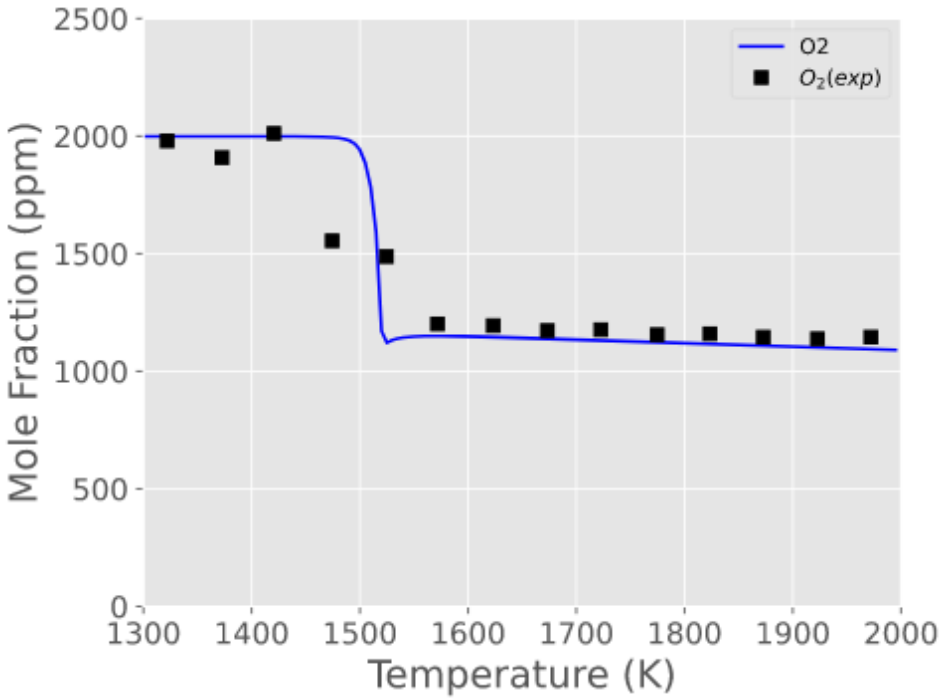

Figure 40. Oxidation of 1000 ppm NH_3 with 2000 ppm O_2 in a PFR. Experimental data[65] and modelling results comparison of O_2 concentration profile. P = 1.27 bar, Φ = 0.375.

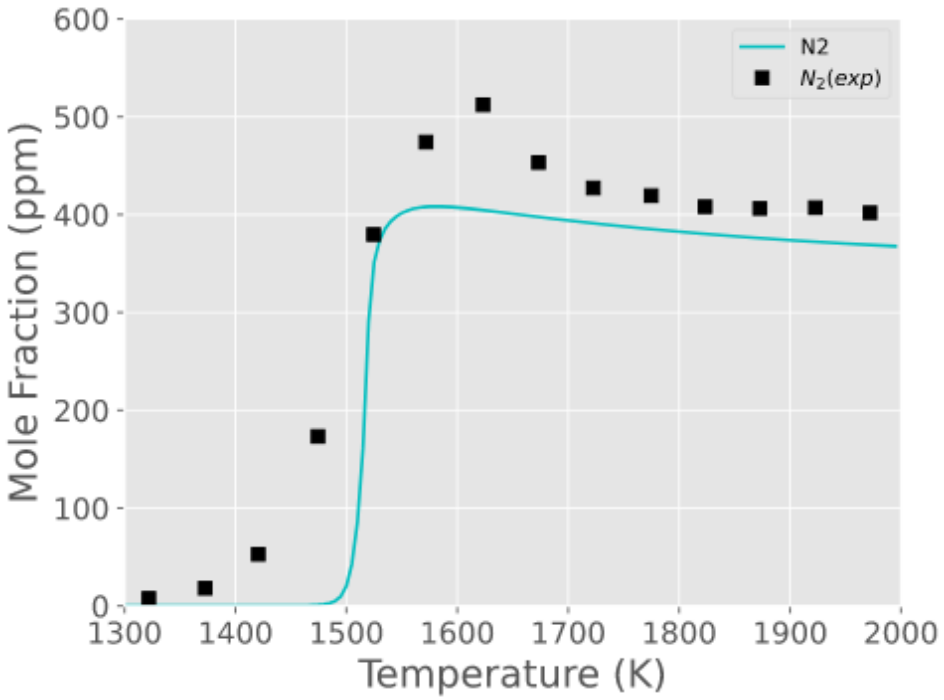

Figure 41. Oxidation of 1000 ppm NH_3 with 2000 ppm O_2 in a PFR. Experimental data[65] and modelling results comparison of N_2 concentration profile. P = 1.27 bar, Φ = 0.375.

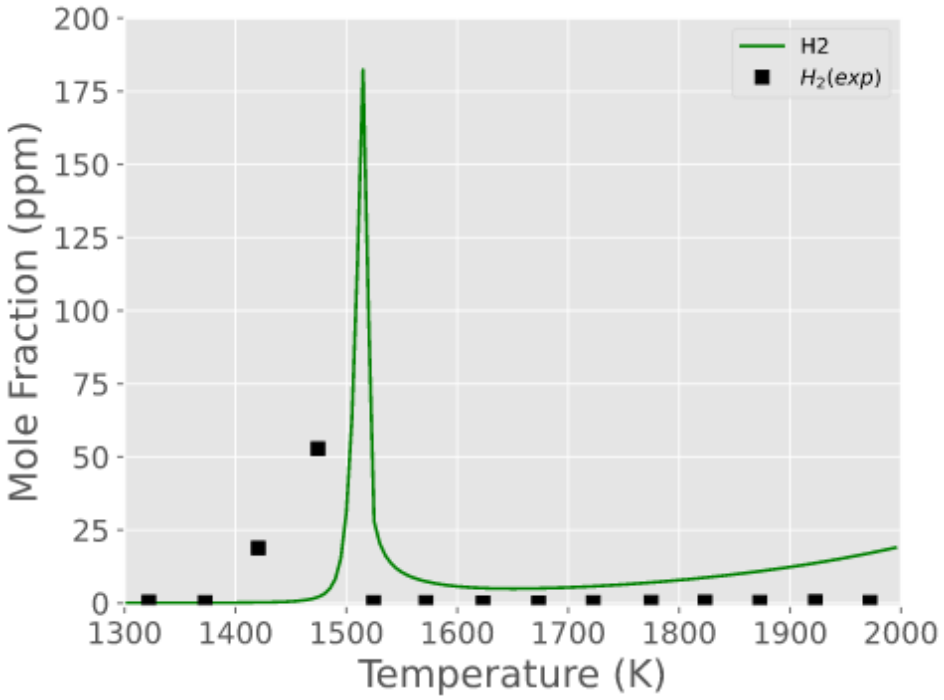

Figure 42. Oxidation of 1000 ppm NH_3 with 2000 ppm O_2 in a PFR. Experimental data[65] and modelling results comparison of H_2 concentration profile. P = 1.27 bar, Φ = 0.375.

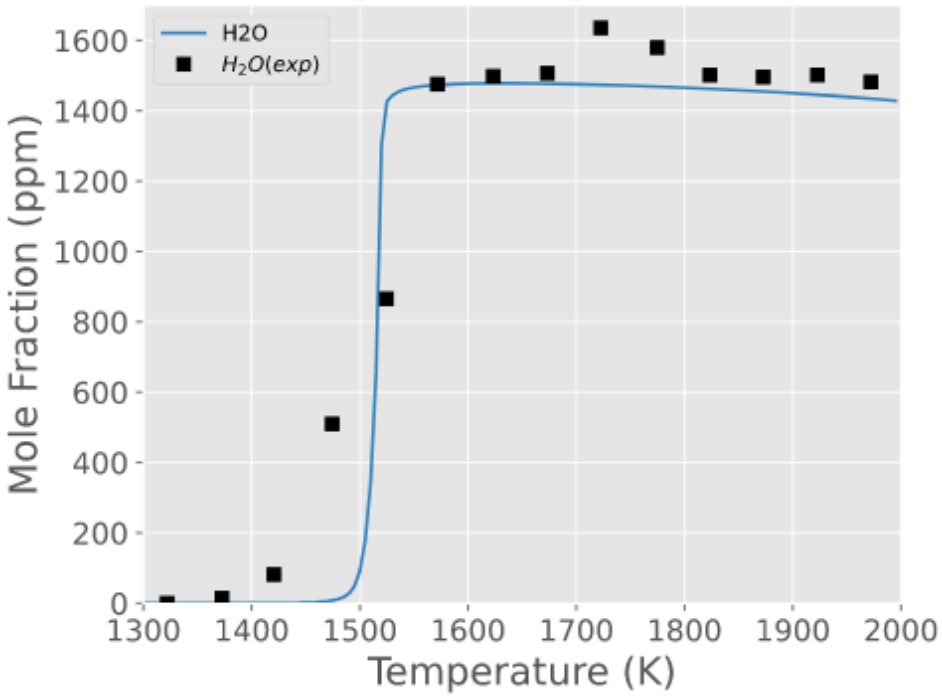

Figure 43. Oxidation of 1000 ppm NH_3 with 2000 ppm O_2 in a PFR. Experimental data[65] and modelling results comparison of H_2O concentration profile. P = 1.27 bar, Φ = 0.375.

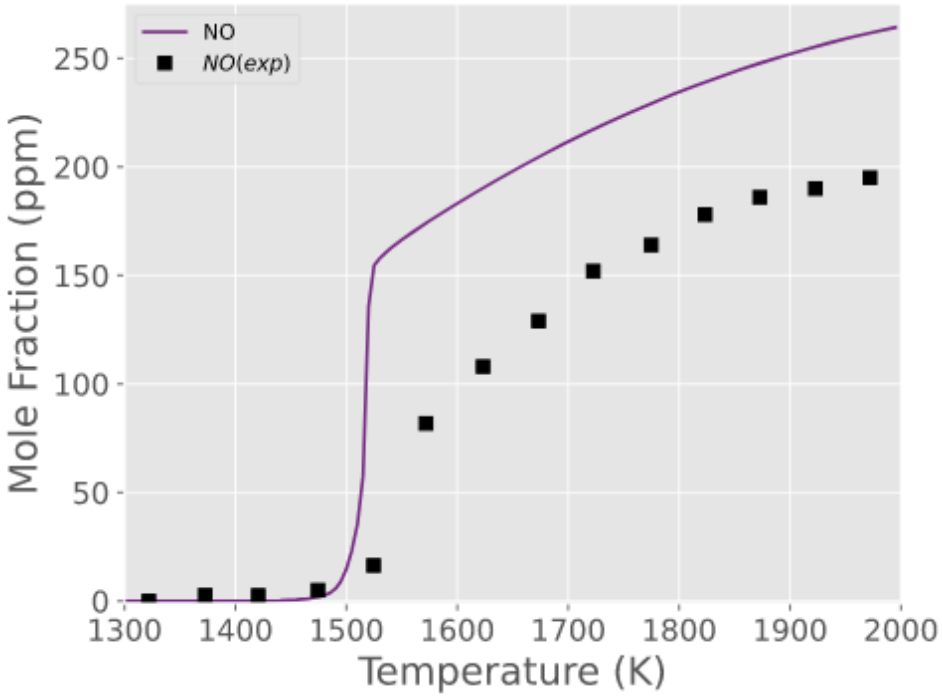

Figure 44. Oxidation of 1000 ppm NH_3 with 2000 ppm O_2 in a PFR. Experimental data[65] and modelling results comparison of NO concentration profile. P = 1.27 bar, Φ = 0.375.

The kinetic model predicts the ignition temperature reasonably well, and consequently, the NH_3, O_2 and H_2O profiles as well. The predicted consumption rate of ammonia and product formation is more abrupt than what the experimental data marks (Figures 39 - 44). The location of the H_2 peak is caught on the same temperature range in the simulation but predicts more mole fractions of H_2 than the values reported in the literature, which are around ~175 ppm and ~60 ppm, respectively. Its worth noting that in this case H_2 was an intermediate species and our simulation predicted accordingly. The onset of NO formation is well reproduced in terms of temperature, as well of N_2. Additionally, the shape and trend of both profiles is well caught, but an overestimation of the NO mole fraction (about 40%) is observed at high temperature.

4.5.5. Jet Stirred Reactor II

4.5.5.1 Stoichiometric conditions

The next benchmarking was done following the experimental set up by Manna et al.[107]. The study was for an oxidation process for a stoichiometric mixture of NH_3 with O_2. The experimental values were obtained at atmospheric pressure and a fixed residence time (τ). The mixtures were diluted in argon, to allow the investigation of N_2 and NO coming exclusively from NH_3. The experimental conditions followed for the simulation are depicted in Table 7. The mixtures were diluted in argon, this is done to allow the investigation of N_2 and NO coming exclusively from NH_3. The experimental conditions followed for the simulation are depicted in Table 13.

Table 13. Conditions used in the simulation of oxidation of NH_3 in a JSR.

Conditions	*Oxidation*
Inlet temperature (T0)	900 – 1350 K
Equivalence ratio (Φ)	1
Residence time (τ)	0.25 s
Pressure	1.2 bar
Diluent (d)	Ar (86%)

The simulation results on the NH_3 oxidation are presented in Figures 45 - 47. In Figure 45 we can see the profiles of N_2 and O_2, with a good representation of the trend of both species throughout most of the studies temperature range. However, it can be observed that the start of consumption of O_2 as well as the production of N2 starts at higher temperatures than observed experimentally.

In Figure 46 shown that our simulation initiates the production of H_2 at much higher temperatures than the experimental data, (~1100 K to ~950 K, respectively). Also, the trend of the simulation is in some disagreement with the literature data. However, the behaviour shown

in the experimental data, of rising, falling and then rising again is somewhat represented by our simulation although, apparently, our model would need higher temperatures to achieve this. The range of concentration is also well represented by the simulation.

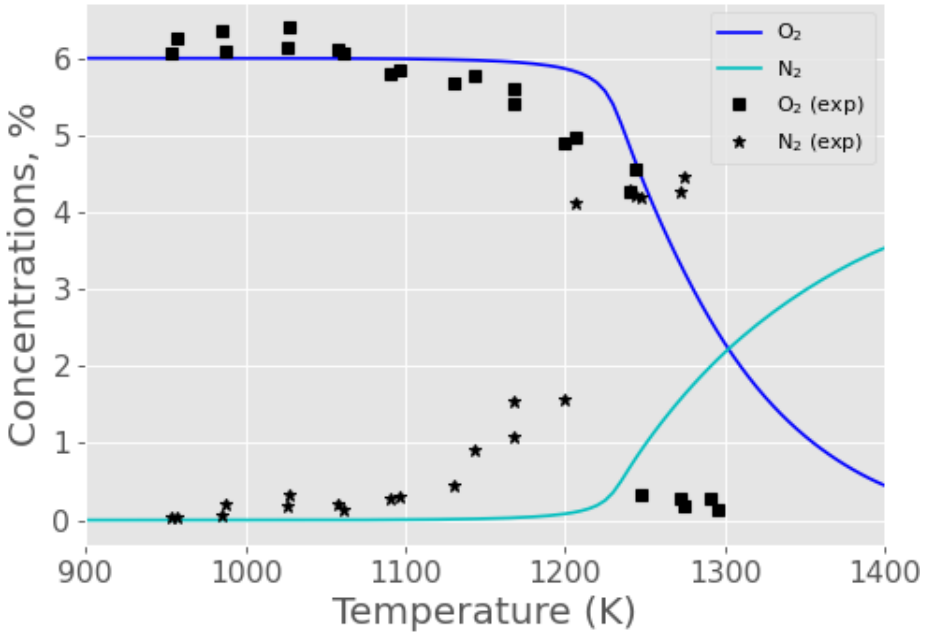

Figure 45. O_2 & N_2 Experimental[107] and simulated concentration profiles, for the oxidation of stoichiometric NH3/O2/Ar (d = 86%) mixtures, at fixed P = 1.2 bar and τ = 0.25 s, in a JSR.

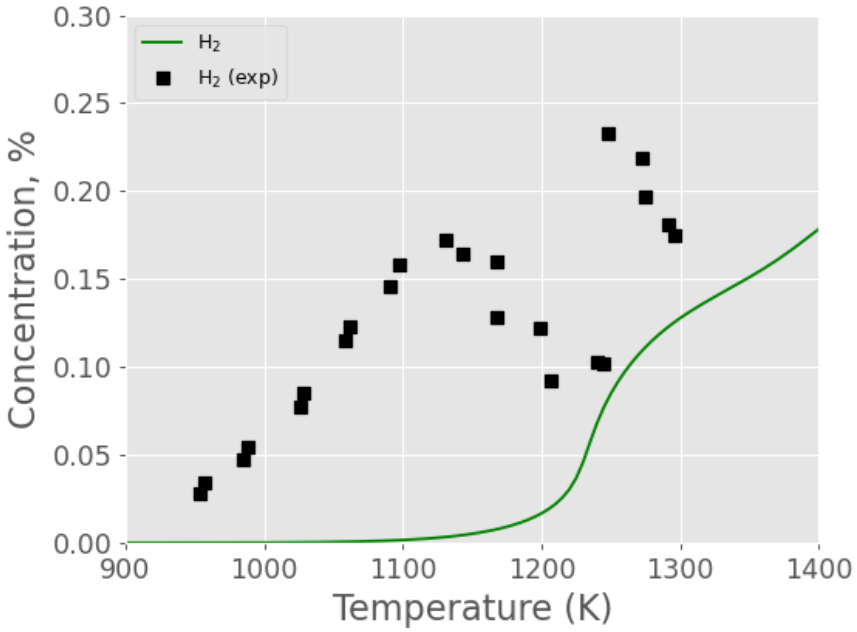

Figure 46. H_2 Experimental[107] and simulated concentration profiles, for the oxidation of stoichiometric NH3/O2/Ar (d = 86%) mixtures, at fixed P = 1.2 bar and τ = 0.25 s, in a JSR.

In the case of NO, although having low concentration values, Figure 50 shows us that the trend and behaviour of NO is well represented by our simulation. Nevertheless, the experimental data achieves almost the double of the concentration than our simulated data.

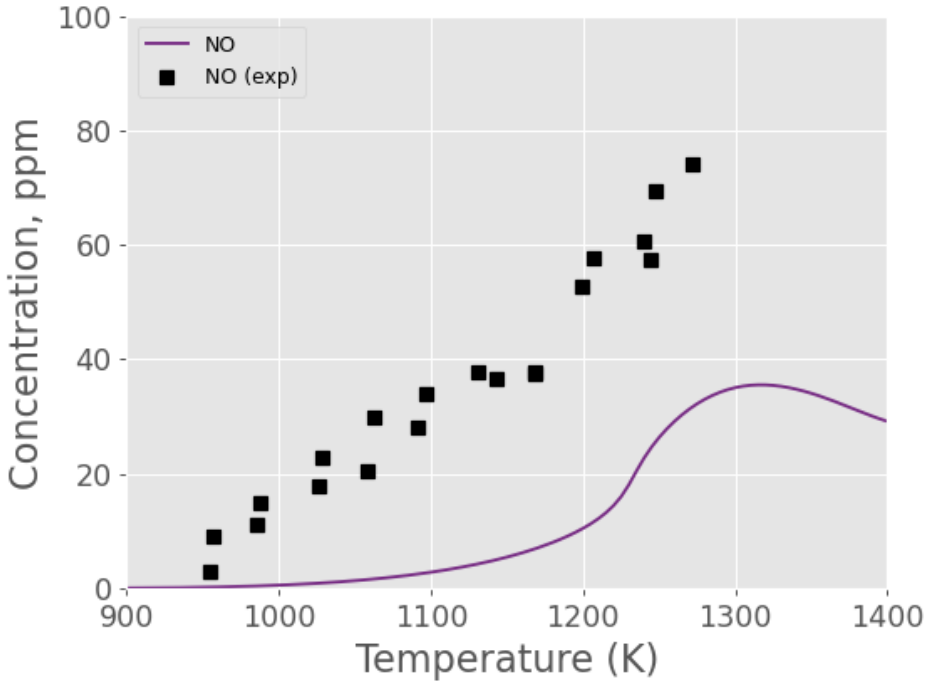

Figure 47. NO Experimental[107] and simulated concentration profiles, for the oxidation of stoichiometric NH3/O2/Ar (d = 86%) mixtures, at fixed P = 1.2 bar and τ = 0.25 s, in a JSR.

Overall, this simulation results shows that we have most behaviours and trends captured correctly, however there is still room for improvement.

4.5.5.2. Rich conditions

This experimental comparison is built upon the previous work conducted by Sabia et al.[107], which bears remarkable similarity to the stoichiometric conditions case. Nonetheless, a key distinction between this case and the prior one[107] lies in the substitution of Ar as the bath gas with N_2, along with a τ value of 0.21 s instead of 0.25 s. The outcomes of this comparison are illustrated in Figures 48 – 50, displaying the simulation outcomes for O_2, H_2, and NO. Notably, in Figure 48, the simulated values of O_2 consumption are represented relatively well in trend and shape relative to the experimental observations.

Figure 49 shows the results for the simulation of the H_2 concentration profile. We see that although the simulation predicted the H_2 concentration rise at higher temperatures than the experimental data, the trend of having a small growth in concentration and then a sudden increase. It is worth noting that the highest point of H_2 concentration for the experimental data is almost ten times larger than the one predicted by the simulation.

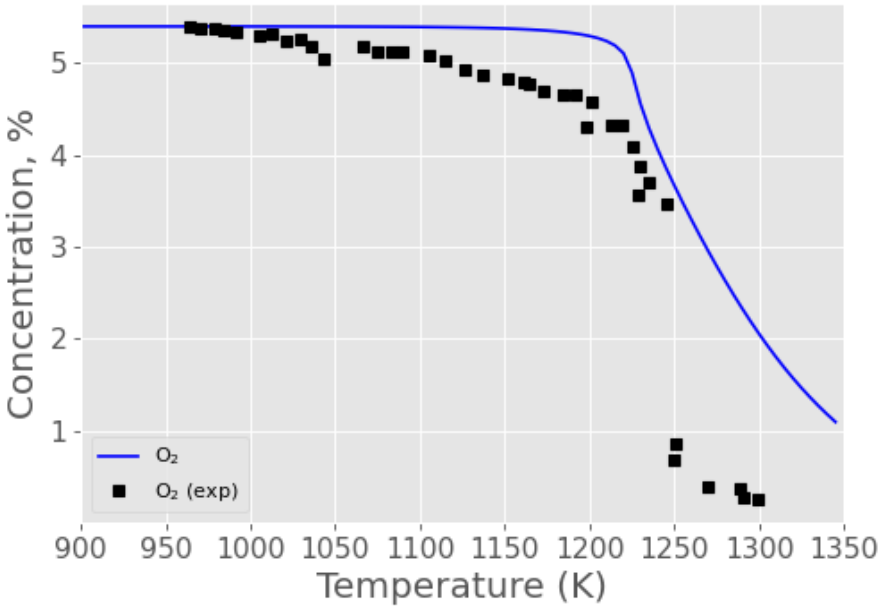

Figure 48. O_2 Experimental and simulated concentration profiles for the oxidation of rich NH_3/O_2 mixtures diluted in N_2 at 86%, at P=1.2 bar and τ = 0.21 s.

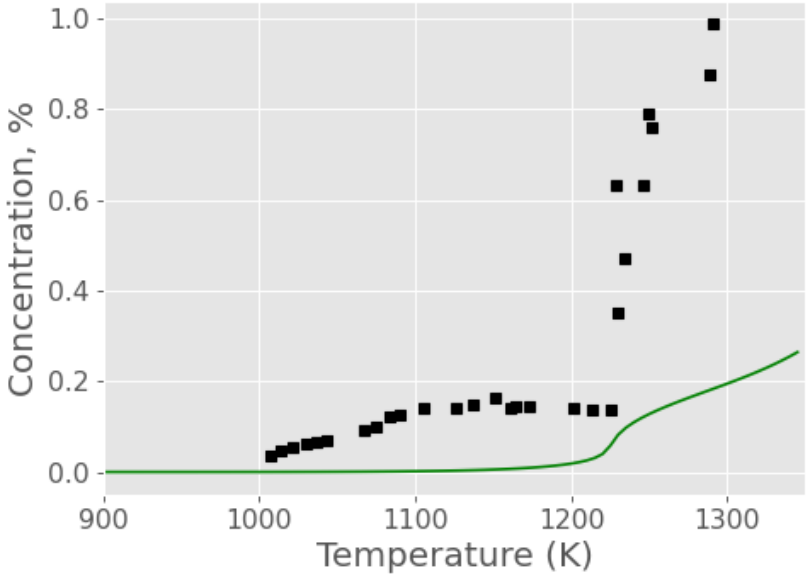

Figure 49. H_2 Experimental and simulated concentration profiles for the oxidation of rich NH_3/O_2 mixtures diluted in N_2 at 86%, at P=1.2 bar and τ = 0.21 s.

In the case of NO, it can be observed in Figure 50 that in this case the initial temperature in which the concentration of NO rises is on lower temperatures compared to Figure 47. Also, the trend and shape of the profile resembles well the experimental data, however, the amount of NO is lower and peaks at higher temperatures than the values shown by the literature.

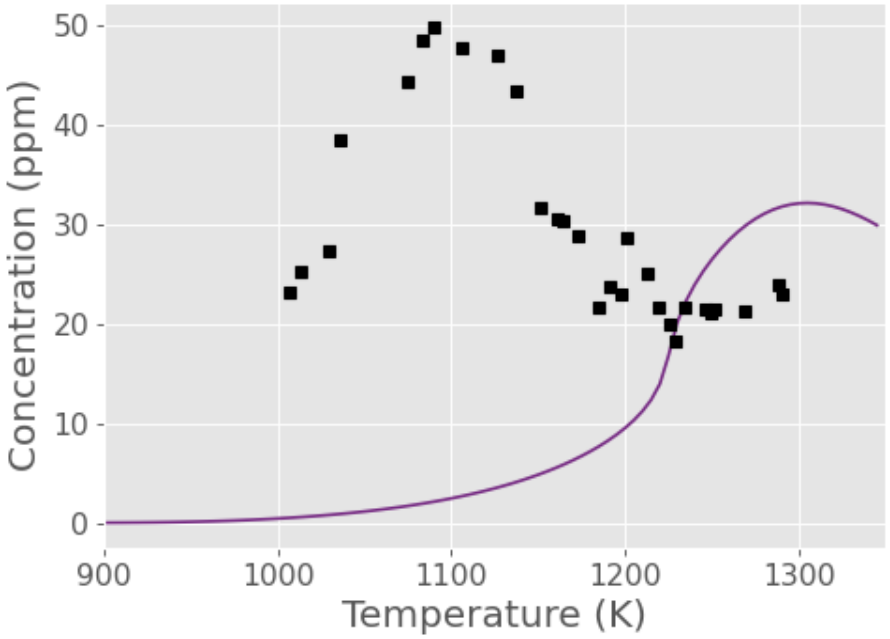

Figure 50. NO Experimental and simulated concentration profiles for the oxidation of rich NH_3/O_2 mixtures diluted in N_2 at 86%, at P=1.2 bar and τ = 0.21 s.

4.5.7. High Pressures

This benchmark simulation was performed using experimental data reported by M.U. Alzueta [66]. The experimental set up consisted of the reactant gases being premixed before entering a quartz flow reactor 153.8 cm (about 5.05 ft) long, with an inner diameter of 6 mm. The aim was to investigate the effect of the main variables: oxygen excess ratio (stoichiometric, λ = 1, and oxidizing, λ = 3, conditions), pressure (10, 20, 30 and 40 bar) and temperature (from 600 to 1275 K) using concentration of ammonia ~ 1000 ppm. The excess ratio (λ) is defined according to the NH_3 oxidation reaction to N2 ($NH_3+0.75O_2 \rightarrow 0.5N_2+1.5H_2O$) according to the equation:

$$\lambda = \frac{(O_2)_{inlet}}{(O_2)_{stoichiometric}} \text{[4.1]}$$

In the experiments, the flow rate was set as 1000 ml (STP)/min, which gives a temperature and pressure dependent gas residence time in the isothermal reaction zone as described in the following equation:

$$t_r(s) = 231.6\frac{P(bar)}{T(K)} \text{[4.2]}$$

Concentrations of NH_3, N_2 and O_2 are simulated and compared to the experimental data provided in the paper[81]. In the following list there is a summary of the experimental initial conditions. The influence of pressure at different temperatures has been evaluated in the 10 to 40 bar range for Φ of 1 and 0.3. All experiments were performed in the 600 – 1275 K temperature interval with a total flow rate of 100 ml (STP)/min and using Ar as bath gas.

4.5.7.1. Stoichiometric conditions

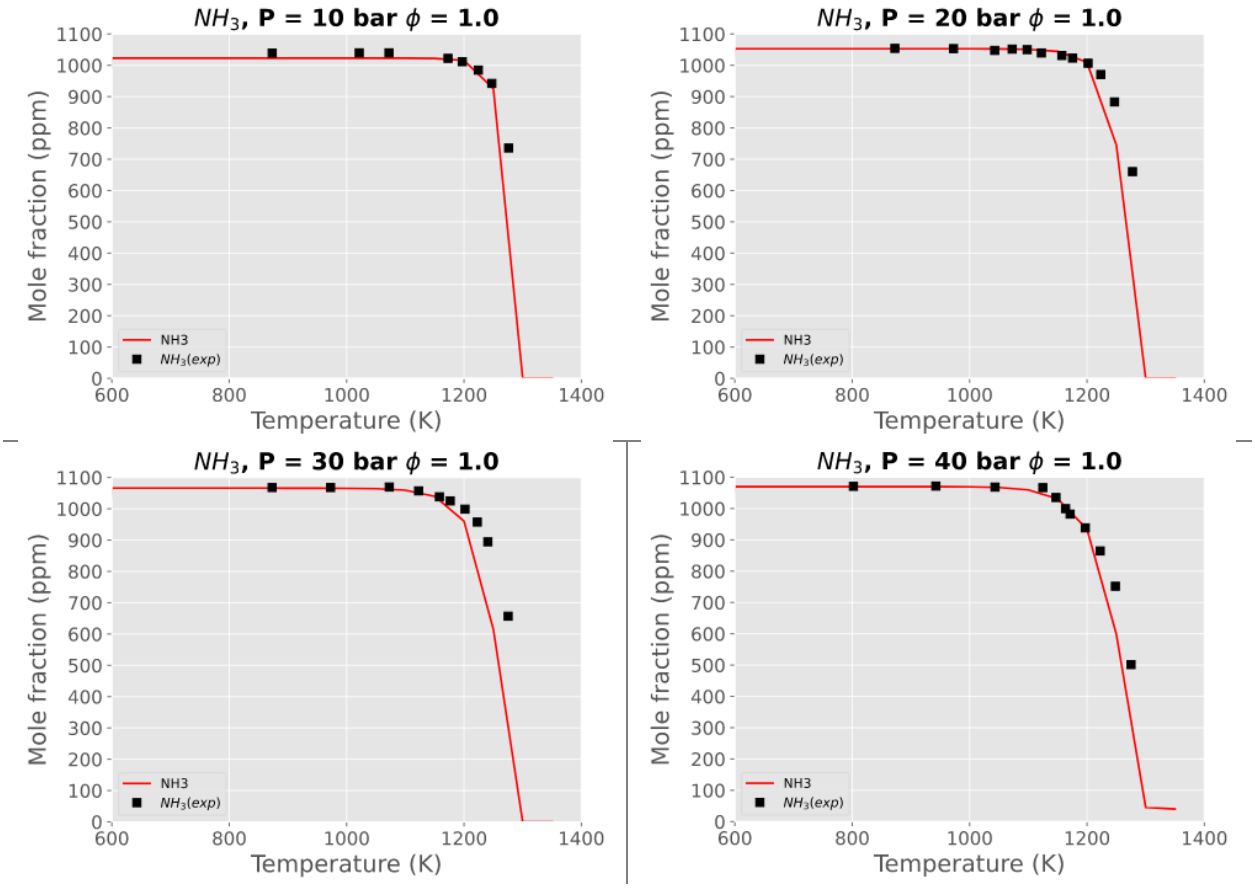

Figure 51. Comparison of experimental[81] and simulated NH3 concentration profiles at 10, 20, 30 and 40 bar, respectively, and Φ = 1.0 using Ar as bath gas.

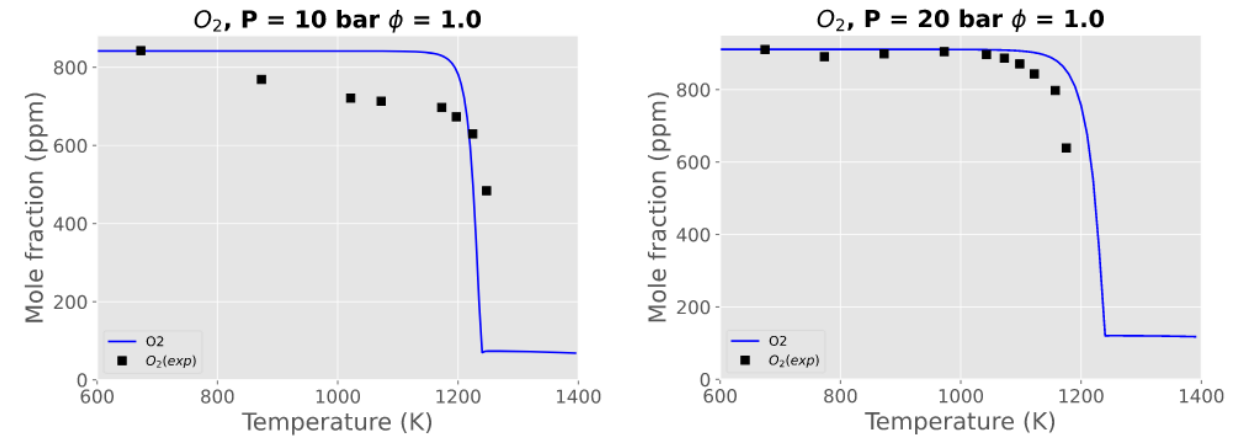

Figure 52. Comparison of experimental[81] and simulated O2 concentration profiles at 10, 20, 30 and 40 bar, respectively, and Φ = 1.0 using Ar as bath gas.

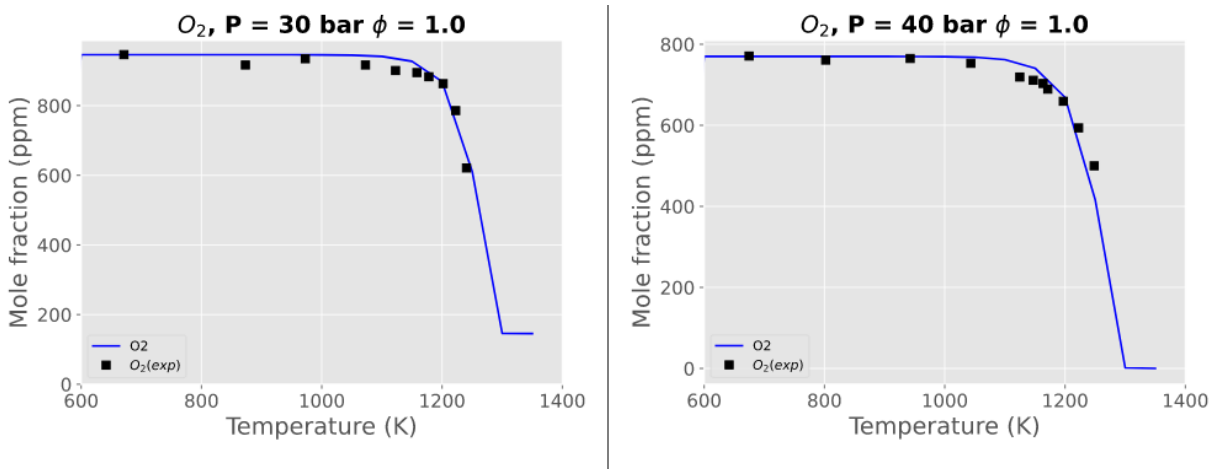

Figure 52. Comparison of experimental[81] and simulated O2 concentration profiles at 10, 20, 30 and 40 bar, respectively, and Φ = 1.0 using Ar as bath gas.

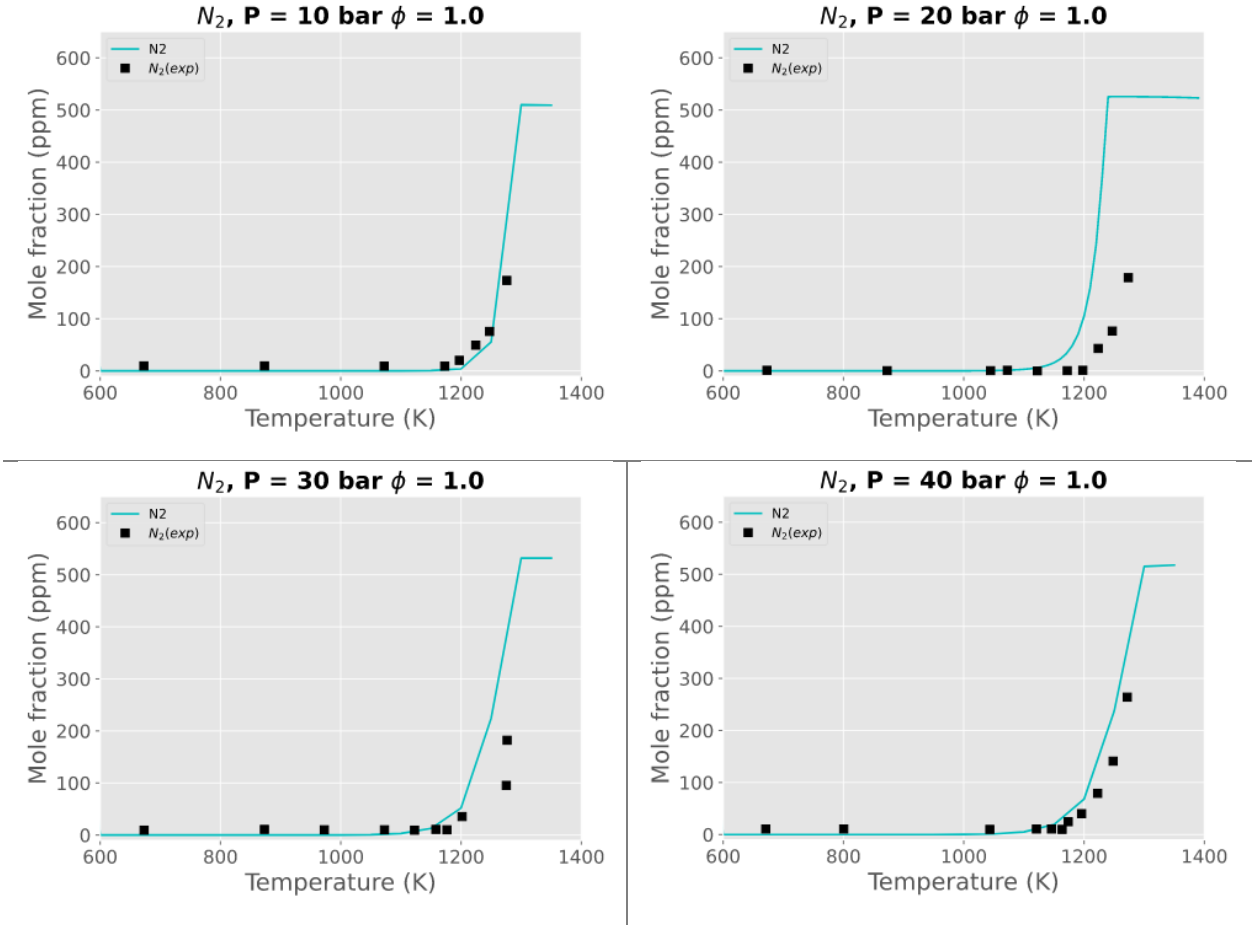

Figure 53. Comparison of experimental[81] and simulated N2 concentration profiles at 10, 20, 30 and 40 bar, respectively, and Φ = 1.0 using Ar as bath gas.

4.5.7.2. Lean conditions

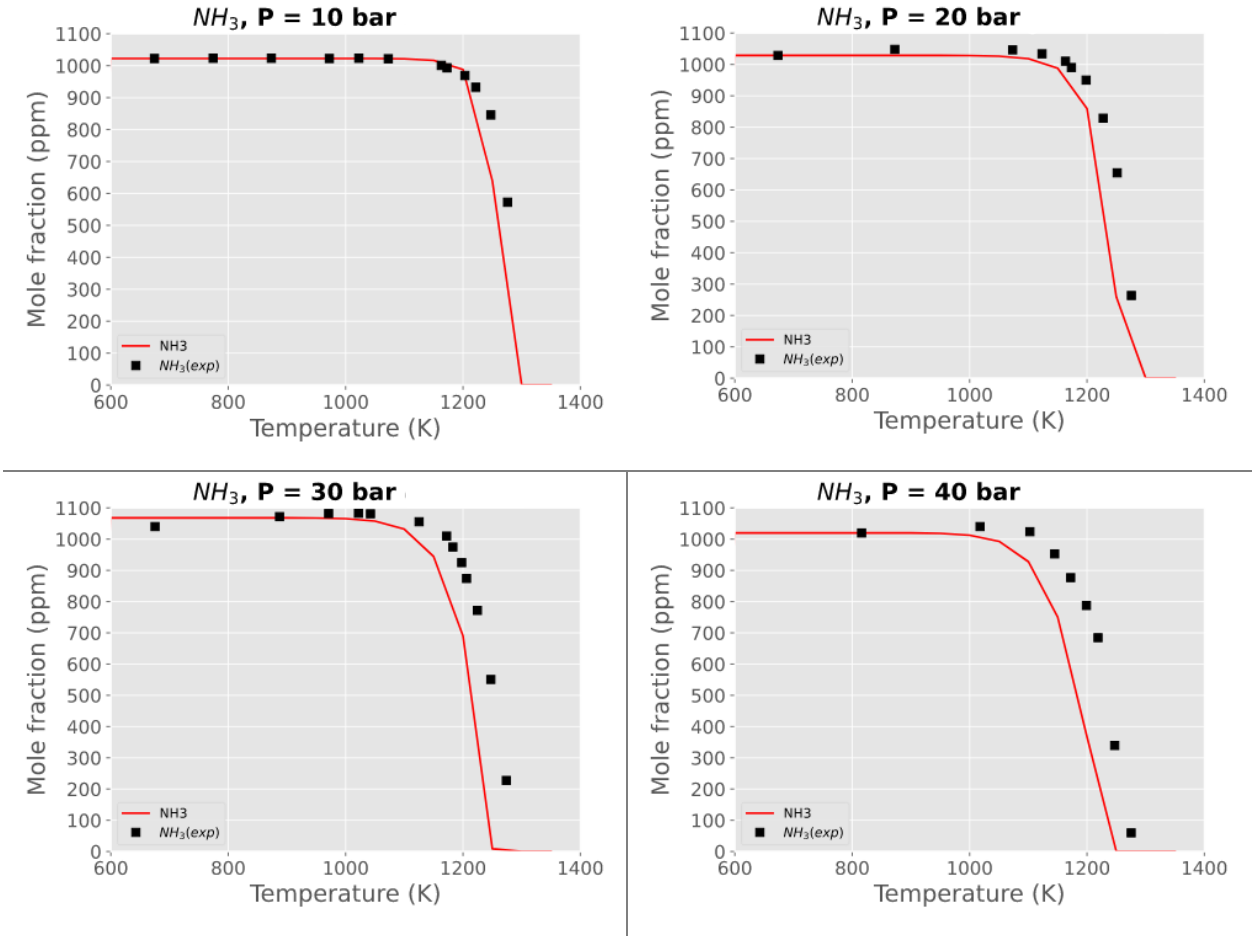

Figure 54. Comparison of experimental[81] and simulated NH3 concentration profiles at 10, 20, 30 and 40 bar, respectively, and a stoichiometric ratio of 0.3 using Ar as bath gas.

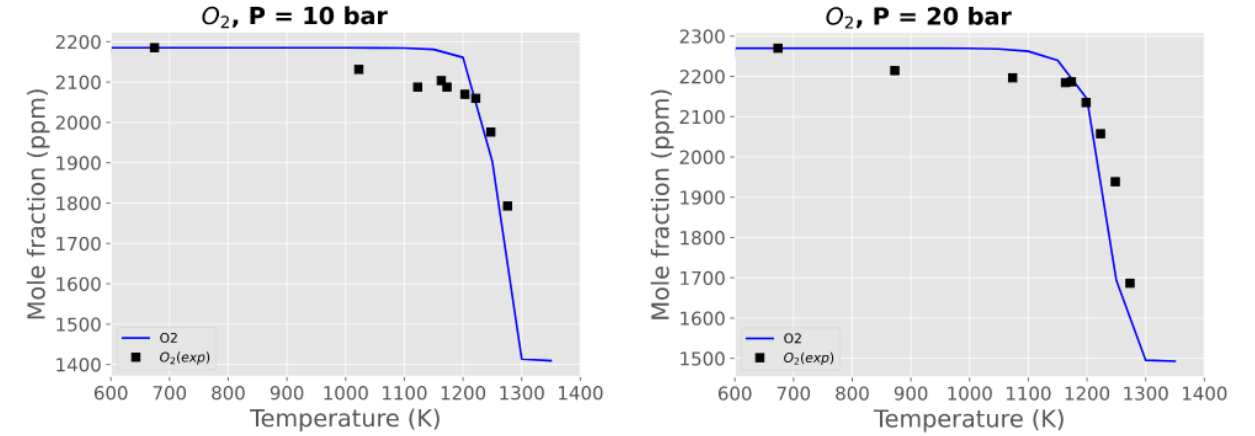

Figure 55. *Comparison of experimental[81] and simulated O2 concentration profiles at 10, 20, 30 and 40 bar, respectively, and a stoichiometric ratio of 0.3 using Ar as bath gas.*

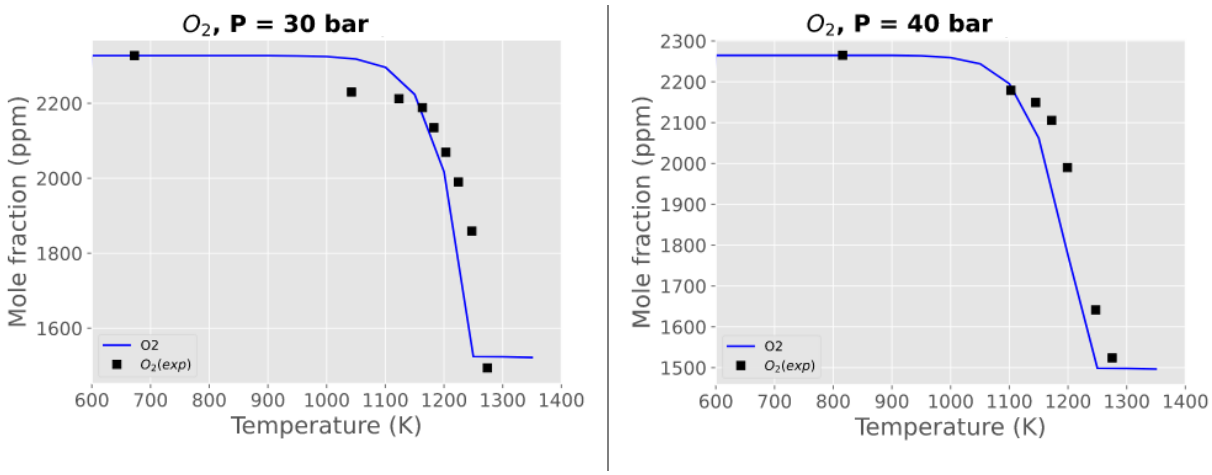

Figure 55. Comparison of experimental[81] and simulated O2 concentration profiles at 10, 20, 30 and 40 bar, respectively, and a stoichiometric ratio of 0.3 using Ar as bath gas.

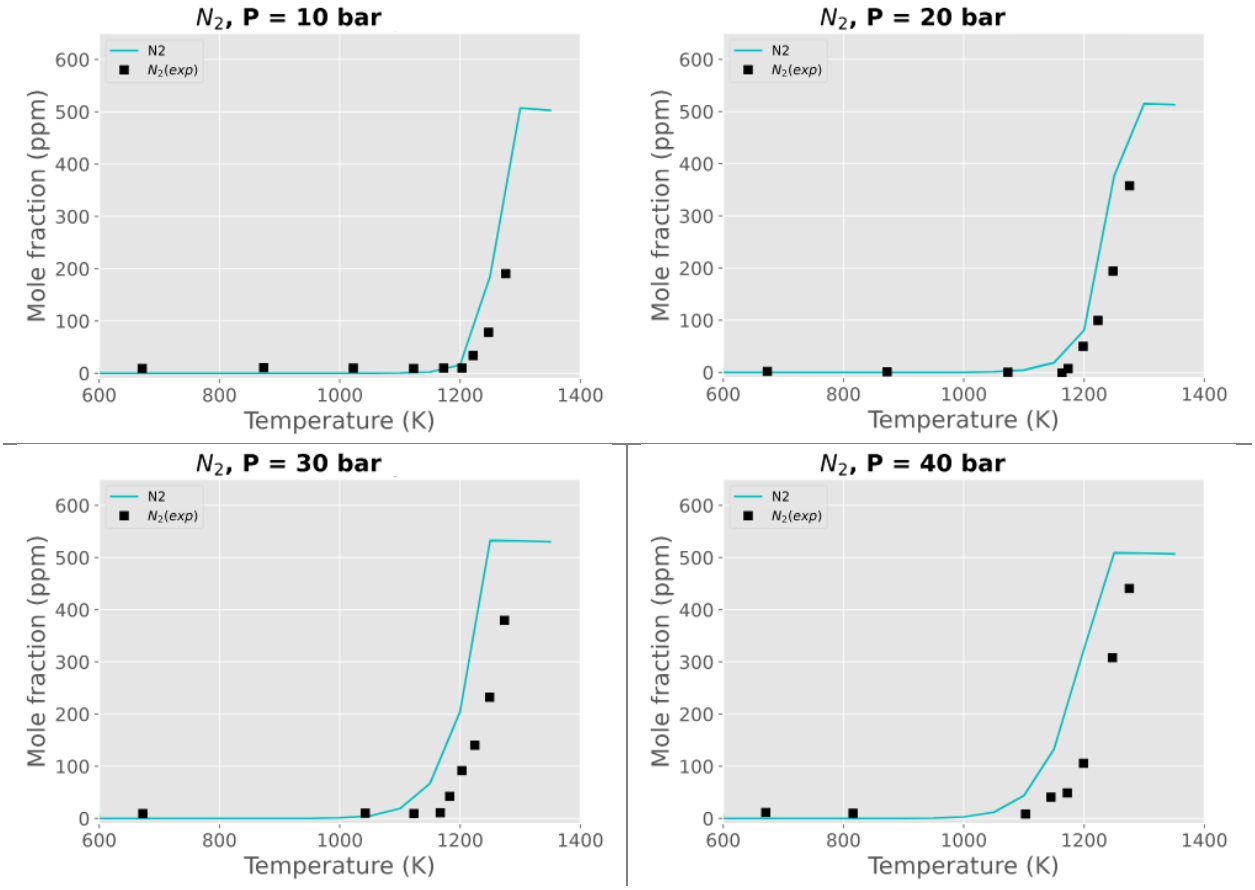

Figure 56. Comparison of experimental[81] and simulated N_2 concentration profiles at 10, 20, 30 and 40 bar, respectively, and a stoichiometric ratio of 0.3 using Ar as bath gas.

The results obtained from all the simulations consistently exhibit a high level of agreement with the corresponding experimental data. Notably, our kinetic model accurately predicts the

behaviour of all species involved in the experimental analysis. The shapes and trends observed in the simulations align closely with the experimental data.

Specifically, when considering the conditions of high pressure, our kinetic model excels in providing a reliable representation of the system. The simulations successfully capture the intricate dynamics and intricate interactions taking place under these elevated pressure conditions. This robust performance underscores the effectiveness and validity of our kinetic model, which proves to be a valuable tool for studying and understanding this system at relatively high pressures.

4.2.1. NH3 with 10% H2

In our research, we embarked upon a study by examining the experimental data performed by Osipova et al.[64] Our objective was to simulate the system described in the paper and compare. The experiments consisted of a flat burner at atmospheric pressure which was used to measure the chemical structure of premixed $NH_3/H_2/O_2$/Ar flames at Φ = 0.8 and Φ = 1.0 at 4.05 bar. The simulation of the flames was done in the same manner. The burner temperature was maintained at 368 K throughout the simulations. The molar composition of each simulation is depicted in Table 14. It also includes the values of the gas velocity at burner surface reported on the experimental data and the one obtained through the simulation.

Table 14. Molar composition of fresh gas blends and flame stabilization conditions in $NH_3/H_2/O_2$/Ar flames.

Φ	P, bar	Reactants mole fraction				Gas velocity at burner surface (cm/s) T_0=368 K	
		NH_3	H_2	O_2	Ar	Exp data	Simulated
0.8	4.05	0.077	0.04	0.121	0.762	7.72	5.542
1.0	4.05	0.082	0.0508	0.1123	0.7549	7.72	9.093

Figures 57 and 58 show the main consumed and produced species in terms of concentration for both the lean and stoichiometric conditions studied, respectively. Our simulated values and the experimental data have significant discrepancies for certain species. Notably, the observed disparities were primarily associated with the consumption of oxygen and water production for the lean case and for the stoichiometric conditions it also included less consumption of hydrogen. However, the quantities of nitrogen remained consistent between our simulation and the experimental data.

An atom balance analysis we performed showed that the experimental data is inconsistent and potentially erroneous, not keeping atom balance for the N and H elements. The implications of this finding raise important questions regarding the accuracy and reliability of the original experimental measurements presented in this experimental work. The observed discrepancies,

with oxygen consumption and water production falling short in our simulation but nitrogen quantities remaining constant, suggest the presence of systematic errors or inaccuracies in the reported experimental data. Further investigation and validation are warranted to ascertain the true nature of the observed inconsistencies and to establish a more accurate representation of the system under study.

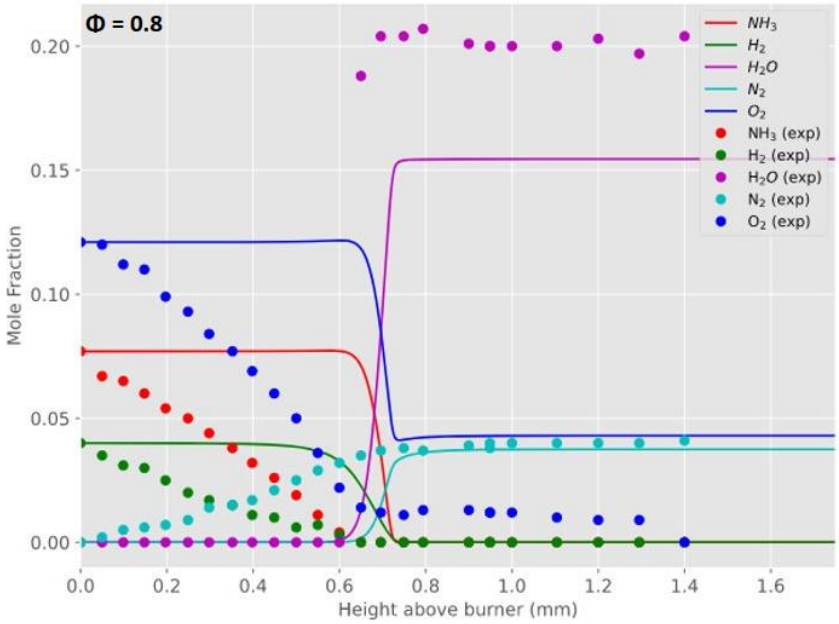

Figure 57. Mole fraction profiles of NH_3, H_2, H_2O, N_2 and O_2 for lean $NH_3/H_2/O_2/Ar$ flames at 4.05 bar.

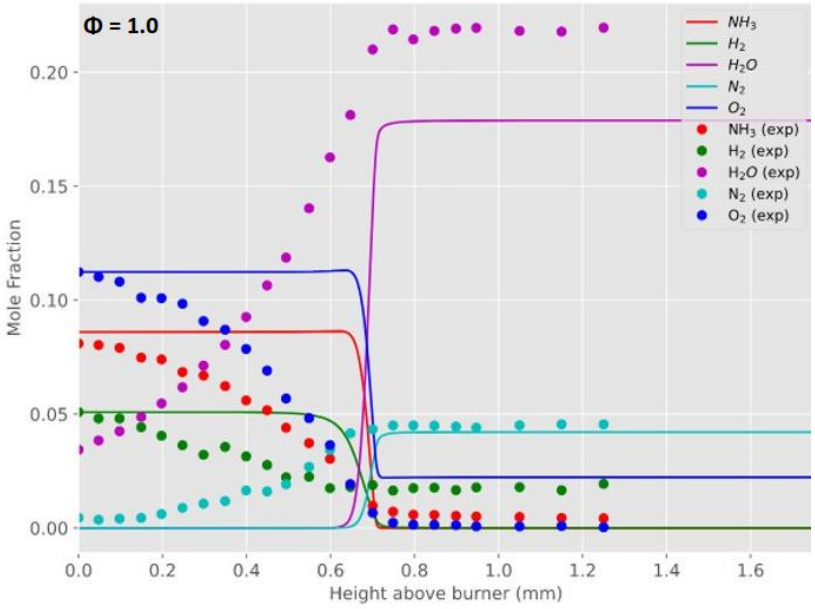

Figure 58. Mole fraction profiles of NH_3, H_2, H_2O, N_2 and O_2 for stoichiometric $NH_3/H_2/O_2/Ar$ flames at 4.05 bar.

Although there are problems in the reported values, these comparisons were fruitful to analyze intermediate and overall species that are not tracked in most papers. The experimental data should be taken with a grain of salt, as noted above. However, a qualitative comparison is still beneficial. In Figures 59 – 72 comparisons between experimental data and simulation results of our model can be observed.

4.5.9.1 Lean conditions Φ = 0.8

Figure 59 shows the comparison between the experimental data and the simulated results of NO. It can be observed that in this case, the prediction of the mole fraction is ~42% smaller compared to the experimental final conversion value. The temperature in which the NO starts to form is higher than the one obtained experimentally[64].

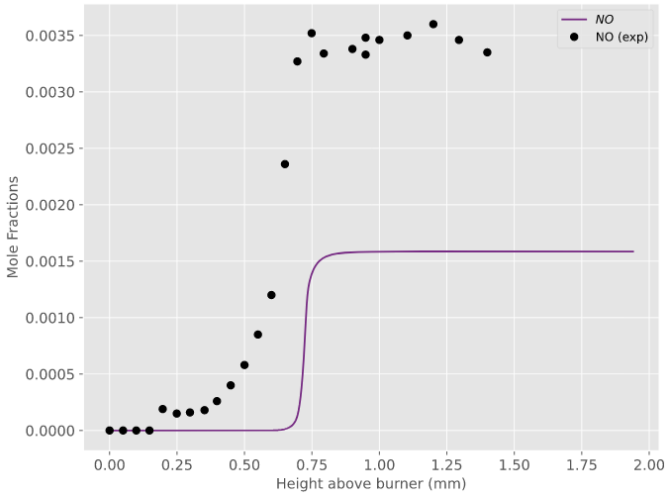

Figure 59. Mole fraction profile comparison of experimental[64] and simulated values of NO for lean (Φ = 0.8) $NH_3/H_2/O_2/Ar$ flames at 4.05 bar.

Figure 60 shows three different plots for the species N2O, the porpoise of this is to showcase the differences and similarities in more depth between the experimental data and the simulation results. Figure 60 A shows the original plot in which the maximum value obtained in our simulation is considerably higher (~0.006) than the reported experimentally (~0.001). Also, the trend between the fraction profiles differs deeply, but this is due to the difference in the values of the peaks. In Figure 60 B the profile obtained experimentally with the simulated one reduced 10 times. This shows that the trend is similar just with a much larger mole fraction value at the maximum point, but the trend is the same and we also get the behaviour of increasing the mole fraction until it starts to decrease and consume all the N_2O. Figure 60 C is a close up on the experimental values compared to the actual size of the simulation results.

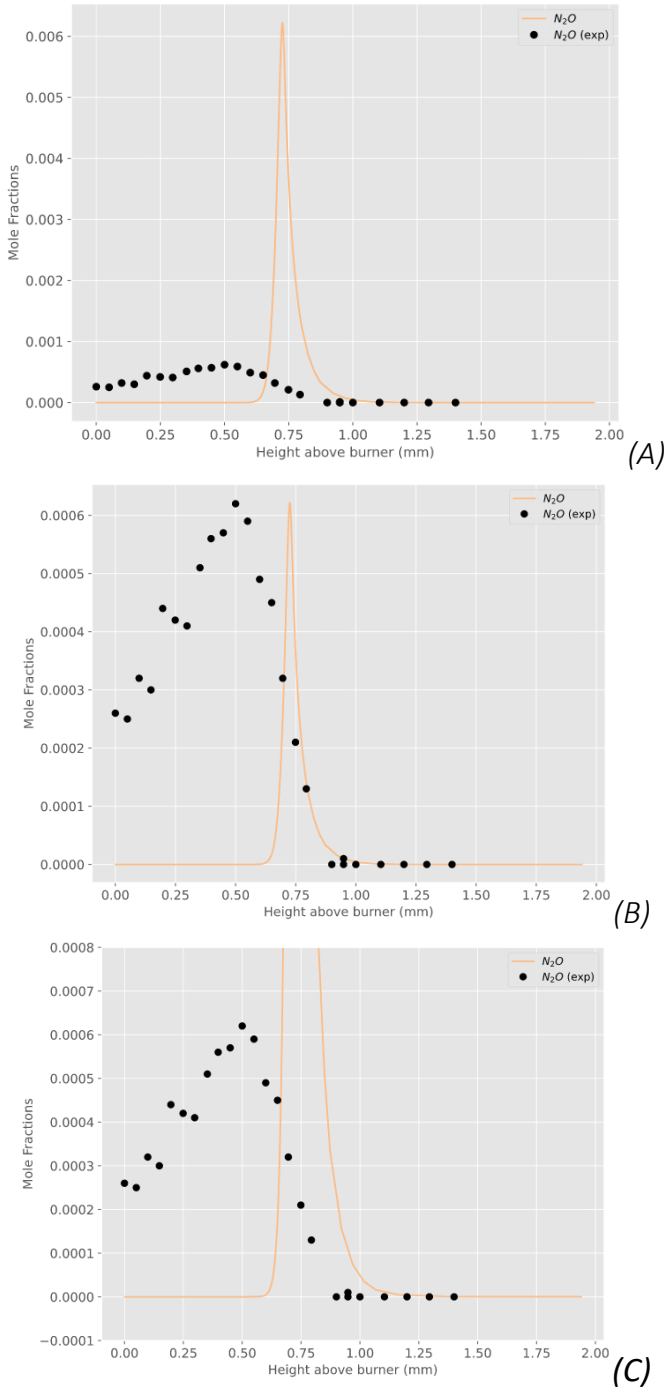

Figure 60. Mole fraction profiles comparison of experimental[64] and simulated values of N_2O for lean (Φ = 0.8) $NH_3/H_2/O_2/Ar$ flames at 4.05 bar. (A) Unmodified fraction profile. (B) Profile reduced 10 times. (C) Unmodified fraction profile close to the experimental data.

Figure 61 shows an odd behaviour by the simulated prediction. The trend of increasing and slowly over the height of the burner decreasing in mole fraction is captured relatively well. However, ~0.75 mm there is an abrupt decrease in the mole fractions that doesn't represent something physically viable.

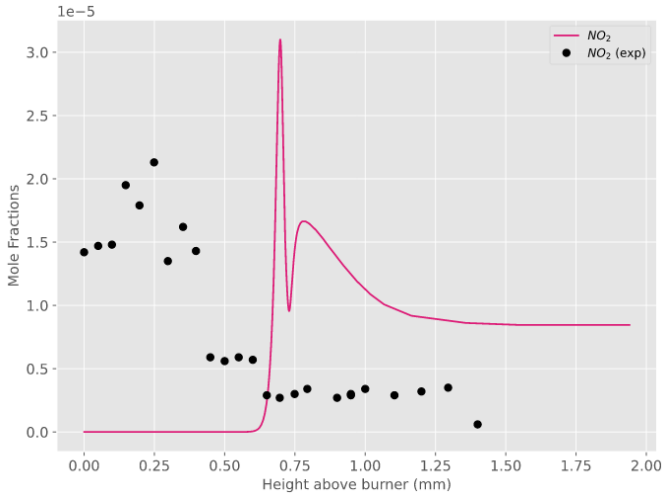

Figure 61. Mole fraction profile comparison of experimental[64] and simulated values of NO_2 for lean (Φ = 0.8) $NH_3/H_2/O_2/Ar$ flames at 4.05 bar.

In the case of the mole fraction profile of H, it can be seen in Figure 62 that our simulation predicted relatively well the behaviour of an intermediate species and the height above the burner at which the maximum peak is reported in the experimental data. However, the value of the mole fraction is considerably lower than the experimental value (~40%).

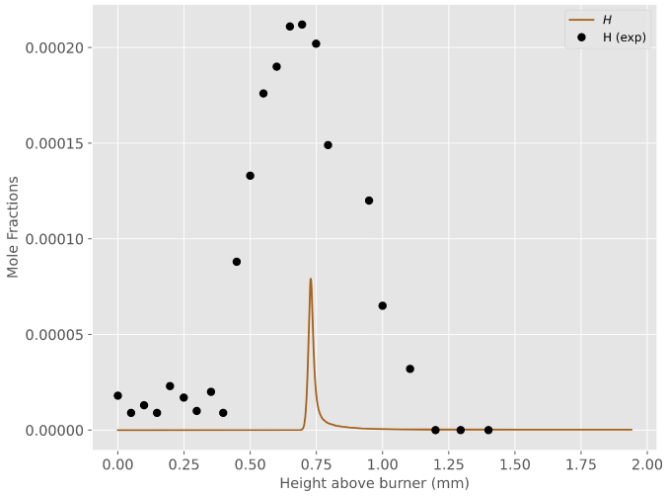

Figure 62. Mole fraction profile comparison of experimental[64] and simulated values of H for lean (Φ = 0.8) $NH_3/H_2/O_2/Ar$ flames at 4.05 bar.

In Figure 63 it can be appreciated that the behaviour and trend of the O profile is relatively well represented by our simulation compared to the experimental values. The results show the peak

of conversion at approximately the same height and mole fraction value and the decrease that comes after is also well predicted.

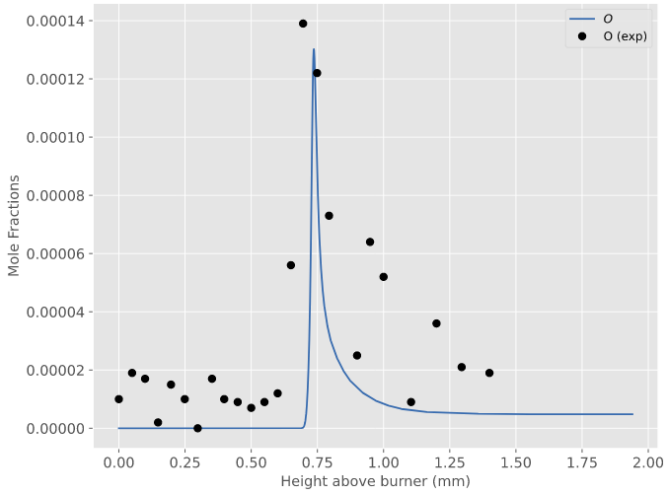

Figure 63. Mole fraction profile comparison of experimental[64] and simulated values of O for lean (Φ = 0.8) $NH_3/H_2/O_2/Ar$ flames at 4.05 bar.

Figure 64 displays the mole fraction profiles for the OH species, showcasing a relatively good representation of the experimental values in the simulation. However, there are some differences worth noting. The conversion values in the simulation appear to be smaller compared to the experimental data, and the decrease after the maximum peak is more abrupt in the simulation.

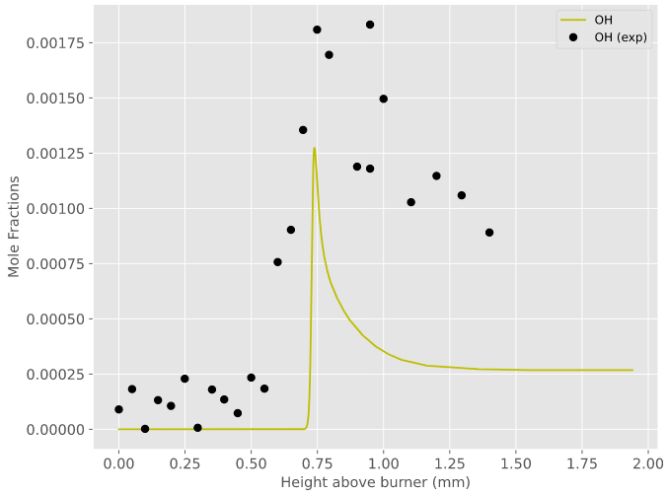

Figure 64. Mole fraction profile comparison of experimental[64] and simulated values e of NO for lean (Φ = 0.8) $NH_3/H_2/O_2/Ar$ flames at 4.05 bar.

Finally, Figure 65 shows the comparison for the NH_2 species, in which a similar trend of being an intermediate species with a short distance in the burner is observed. However, the results

predicted by our simulation are at a larger height above the burner and a considerably higher value of the maximum peak of conversion.

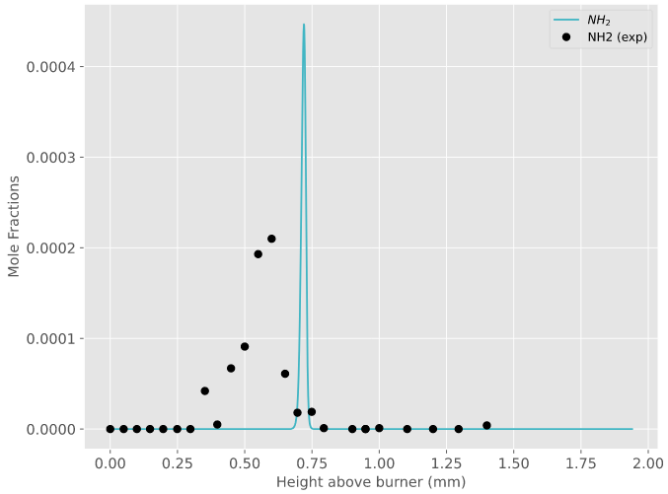

Figure 65. Mole fraction profile comparison of experimental[64] and simulated values of NH_2 for lean (Φ = 0.8) $NH_3/H_2/O_2/Ar$ flames at 4.05 bar.

4.2.2. Stoichiometric conditions Φ = 1.0

Under stoichiometric conditions, we present the species that exhibited significant changes throughout the simulation. Species that do not appear in this section retained consistent trends during the simulation. Figure 66 shows the mole profiles for NO, and we can see a reasonable improvement in the prediction of the amount of NO.

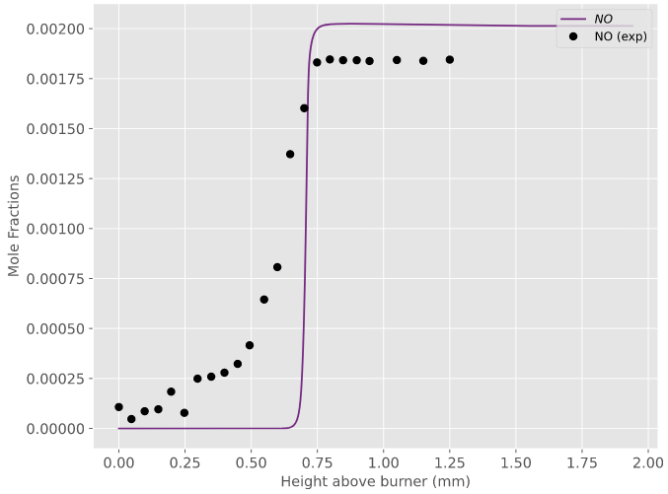

Figure 66. Mole fraction profile comparison of experimental[64] and simulated values of NO for stoichiometric (Φ = 1.0) $NH_3/H_2/O_2/Ar$ flames at 4.05 bar.

Figure 67 shows that although the simulation results maintain the intermediate species behaviour, shown previously in Figure 62. However, the experimental values for stoichiometric conditions showcase a different behaviour not decreasing to zero the value of mole fraction. Although, it's worth noting that the experimental values reported are too small to generate conclusions.

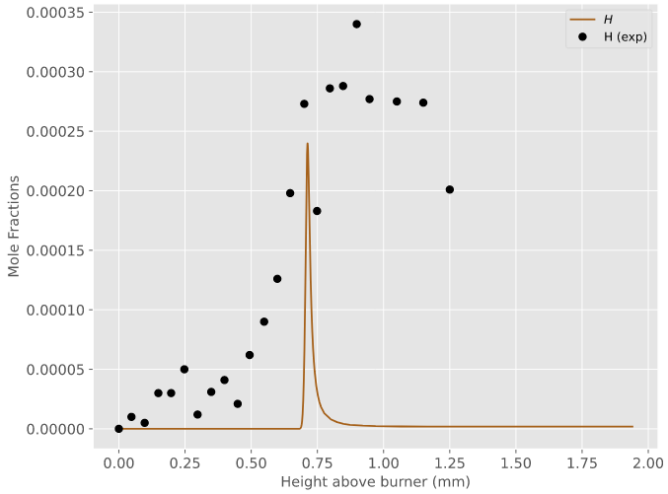

Figure 67. Mole fraction profile comparison of experimental[64] and simulated values of H for stoichiometric (Φ = 1.0) $NH_3/H_2/O_2/Ar$ flames at 4.05 bar.

Figures 67 – 70 show the profiles for O and OH, respectively. In these two cases, the simulated values have increased considerably compared to the experimental values. In fact, for the O profiles, the experimental mole fraction value decreased from ~0.00014 to ~0.00005 and the simulated mole fraction results increased from ~0.00014 to ~0.00025. However, the trend is considerably well represented in both cases.

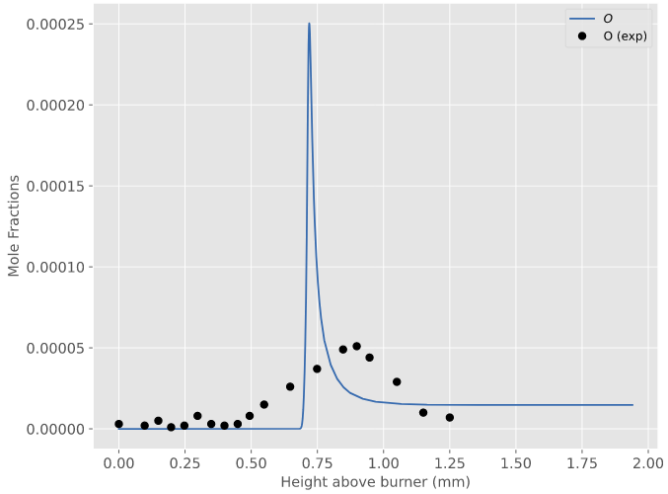

Figure 68. Mole fraction profile comparison of experimental[64] and simulated values of O for stoichiometric (Φ = 1.0) $NH_3/H_2/O_2/Ar$ flames at 4.05 bar.

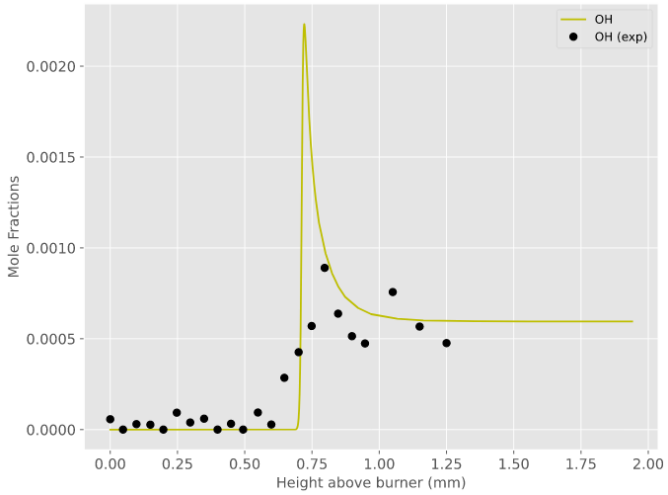

Figure 69. Mole fraction profile comparison of experimental[64] and simulated values of OH for stoichiometric (Φ = 1.0) $NH_3/H_2/O_2$/Ar flames at 4.05 bar.

Figure 70 shows the mole fraction profiles for NH_2, showing a well fit of the results with the experimental data. The simulation represents well the trend and behaviour as well as the value of the maximum peak of the amount of NH_2 created. The increase and decrease in the mole profile aligns with the previous results showing that its an intermediate species.

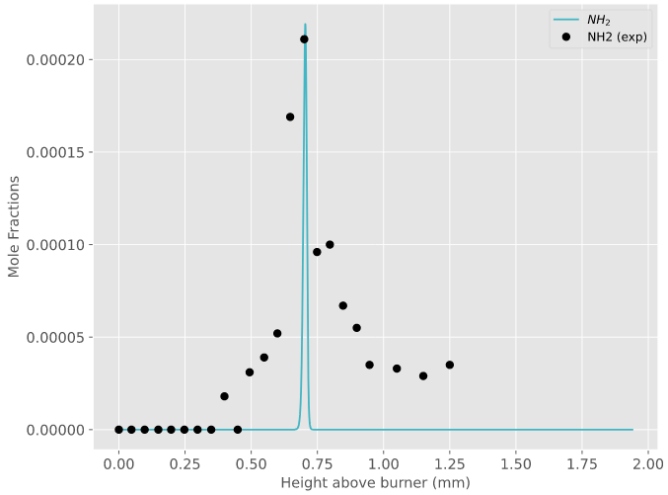

Figure 70. Mole fraction profile comparison of experimental[64] and simulated values of NH_2 for stoichiometric (Φ = 1.0) $NH_3/H_2/O_2$/Ar flames at 4.05 bar.

5. Conclusions

This work presents the first automatically generated predictive chemical kinetic model for ammonia oxidation with and without hydrogen as an additive. The current state of literature models is unsatisfactory: alarming disagreements exist in thermodynamic parameters as well as in some reaction rate constants. In the recent five years (2018-2023) 18 different chemical kinetic models for NH_3 oxidation were published. This plethora of models does not show the community understands NH_3 combustion, but on the contrary, that it still did not come up with a consistent predictive model.

We see the present work within the MIT-PP framework as revolutionary both to the specific field of modelling ammonia oxidation, as well as to the larger chemical kinetic community. It serves as an alarming mirror for the community, highlighting fundamental flaws in the current approach where parameters are modified per study, and often many model parameters are not justified. In our analysis we show the large discrepancy in parameters used in the current literature models and suggest a way forward.

We suggest a consistent set of thermodynamic and kinetic parameters to be adopted by the community. At the very least, we expect that future works will justify any modification they make to these suggested parameters. We performed high level electronic structure computations to achieve a consistent set of thermo-kinetic values to be used in the model. Our model predicts satisfactorily experimental observations. We intend to finalize this fundamental model and publish it soon.

References

(1) on Climate Change (IPCC), I. P. Synthesis Report fd the IPCC Sixth Assessment Report (AR6). https://www.ipcc.ch/report/ar6/syr/, 2023.

(2) Change, U. N. C. The Paris Agreement. https://unfccc.int/process-and-meetings/the-paris-agreement, 2015.

(3) Grinberg Dana, A.; Elishav, O.; Bardow, A.; Ster, G. E.; Grader, G. S. Nitrogen-Based Fuels: A Power-to-Fuel-to-Power Analysis. *Angewandte Chemie International Edition* **2016**, *55*, 8798–8805.

(4) Herbinet, O.; Bartocci, P.; Grinberg Dana, A. On the use of ammonia as a fuel – A perspective. *Fuel Communications* **2022**, *11*, 100064.

(5) Elishav, O.; Mosevitzky Lis, B.; Miller, E. M.; Arent, D. J.; Valera-Medina, A.; Grinberg Dana, A.; Shter, G. E.; Grader, G. S. Progress and Prospective of Nitrogen-Based Alternative Fuels. *Chemical Reviews* **2020**, *120*, 5352–5436.

(6) Elbaz, A. M.; Wang, S.; Guiberti, T. F.; Roberts, W. L. Review on the recent advances on ammonia combustion from the fundamentals to the applications. *Fuel Communications* **2022**, *10*, 100053.

(7) Blarigan, P. V. Advanced internal combustion engine research. *DOE Hydrogen Program Review NREL-CP-570-28890* **2000**, 1–19.

(8) Christensen, C. H.; Johannessen, T.; Sørensen, R. Z.; Nørskov, J. K. Towards an ammonia-mediated hydrogen economy? *Catalysis Today* **2006**, *111*, 140–144, Frontiers in Catalysis: A Molecular View of Industrial Catalysis.

(9) Feibelman, P. J.; Stumpf, R. Comments on potential roles of ammonia in a hydrogen economy—a study of issues related to the use of ammonia for on-

board vehicular hydrogen storage. https://www.pc.gov.au/inquiries/completed/climate-change-adaptation/submissions/sub046-attachment7.pdf, 2006.

(10) Law, C. *Combustion physics*; Cambridge university press, 2010.

(11) Zhang, M.; An, Z.; Wang, L.; Wei, X.; Jianayihan, B.; Wang, J.; Huang, Z.; Tan, H. The regulation effect of methane and hydrogen on the emission characteristics of ammonia/air combustion in a model combustor. *International Journal of Hydrogen Energy* **2021**, *46*, 21013–21025.

(12) Kumar, P.; Meyer, T. R. Experimental and modeling study of chemical-kinetics mechanisms for H2–NH3–air mixtures in laminar premixed jet flames. *Fuel* **2013**, *108*, 166–176.

(13) Xiao, H.; Valera-Medina, A. Chemical Kinetic Mechanism Study on Premixed Combustion of Ammonia/Hydrogen Fuels for Gas Turbine Use. *Journal of Engineering for Gas Turbines and Power* **2017**, *139*, 081504.

(14) Pacheco, G. P.; Rocha, R. C.; Franco, M. C.; Mendes, M. A. A.; Fernandes, E. C.; Coelho, P. J.; Bai, X.-S. Experimental and Kinetic Investigation of Stoichiometric to Rich NH3/H2/Air Flames in a Swirl and Bluff-Body Stabilized Burner. *Energy & Fuels* **2021**, *35*, 7201–7216.

(15) Han, L.; Li, J.; Zhao, D.; Xi, Y.; Gu, X.; Wang, N. Effect analysis on energy conversion enhancement and NOx emission reduction of ammonia/hydrogen fuelled wavy micro-combustor for micro-thermophotovoltaic application. *Fuel* **2021**, *289*, 119755.

(16) Chen, J.; Jiang, X.; Qin, X.; Huang, Z. Effect of hydrogen blending on the high temperature auto-ignition of ammonia at elevated pressure. *Fuel* **2021**, *287*, 119563.

(17) Lhuillier, C.; Brequigny, P.; Contino, F.; Mounaïm-Rousselle, C. Experimental study

on ammonia/hydrogen/air combustion in spark ignition engine conditions. *Fuel* **2020**, *269*, 117448.

(18) da Rocha, R. C.; Costa, M.; Bai, X.-S. Chemical kinetic modelling of ammonia/hydrogen/air ignition, premixed flame propagation and NO emission. *Fuel* **2019**, *246*, 24–33.

(19) Goldmann, A.; Dinkelacker, F. Approximation of laminar flame characteristics on premixed ammonia/hydrogen/nitrogen/air mixtures at elevated temperatures and pressures. *Fuel* **2018**, *224*, 366–378.

(20) Mørch, C.; Bjerre, A.; Gøttrup, M.; Sorenson, S.; Schramm, J. Ammonia/hydrogen mixtures in an SI-engine: Engine performance and analysis of a proposed fuel system. *Fuel* **2011**, *90*, 854–864.

(21) Mei, B.; Ma, S.; Zhang, Y.; Zhang, X.; Li, W.; Li, Y. Exploration on laminar flame propagation of ammonia and syngas mixtures up to 10 atm. *Combustion and Flame* **2020**, *220*, 368–377.

(22) Li, R.; Konnov, A. A.; He, G.; Qin, F.; Zhang, D. Chemical mechanism development and reduction for combustion of NH3/H2/CH4 mixtures. *Fuel* **2019**, *257*, 116059.

(23) Sun, Y.; Cai, T.; Zhao, D. Thermal performance and NOx emission characteristics studies on a premixed methane-ammonia-fueled micro-planar combustor. *Fuel* **2021**, *291*, 120190.

(24) Shu, T.; Xue, Y.; Zhou, Z.; Ren, Z. An experimental study of laminar ammonia/methane/air premixed flames using expanding spherical flames. *Fuel* **2021**, *290*, 120003.

(25) Oh, S.; Park, C.; Kim, S.; Kim, Y.; Choi, Y.; Kim, C. Natural gas–ammonia dual-

fuel combustion in spark-ignited engine with various air–fuel ratios and split ratios of ammonia under part load condition. *Fuel* **2021**, *290*, 120095.

(26) Okafor, E. C.; Yamashita, H.; Hayakawa, A.; Somarathne, K. K. A.; Kudo, T.; Tsujimura, T.; Uchida, M.; Ito, S.; Kobayashi, H. Flame stability and emissions characteristics of liquid ammonia spray co-fired with methane in a single stage swirl combustor. *Fuel* **2021**, *287*, 119433.

(27) Xiao, H.; Lai, S.; Valera-Medina, A.; Li, J.; Liu, J.; Fu, H. Study on counterflow premixed flames using high concentration ammonia mixed with methane. *Fuel* **2020**, *275*, 117902.

(28) Filipe Ramos, C.; Rocha, R. C.; Oliveira, P. M.; Costa, M.; Bai, X.-S. Experimental and kinetic modelling investigation on NO, CO and NH3 emissions from NH3/CH4/air premixed flames. *Fuel* **2019**, *254*, 115693.

(29) Jójka, J.; Ślefarski, R. Dimensionally reduced modeling of nitric oxide formation for premixed methane-air flames with ammonia content. *Fuel* **2018**, *217*, 98–105.

(30) Samu, V.; Varga, T.; Rahinov, I.; Cheskis, S.; Turányi, T. Determination of rate parameters based on NH2 concentration profiles measured in ammonia-doped methane–air flames. *Fuel* **2018**, *212*, 679–683.

(31) Zietz, U.; Baumgärtel, G. The laminar flame speeds of propane-ammonia-air mixtures. *Combustion and Flame* **1969**, *13*, 329–330.

(32) Bockhorn, H.; Fetting, F.; Mende, J. The laminar flame velocities of propane/ammonia mixtures. *Combustion and Flame* **1972**, *18*, 471–473.

(33) Gross, C. W.; Kong, S.-C. Performance characteristics of a compression-ignition engine using direct-injection ammonia–DME mixtures. *Fuel* **2013**, *103*, 1069–1079.

(34) Ryu, K.; Zacharakis-Jutz, G. E.; Kong, S.-C. Performance characteristics of compression-ignition engine using high concentration of ammonia mixed with dimethyl ether. *Applied Energy* **2014**, *113*, 488–499.

(35) Wang, Z.; Han, X.; He, Y.; Zhu, R.; Zhu, Y.; Zhou, Z.; Cen, K. Experimental and kinetic study on the laminar burning velocities of NH3 mixing with CH3OH and C2H5OH in premixed flames. *Combustion and Flame* **2021**, *229*, 111392.

(36) Li, M.; He, X.; Hashemi, H.; Glarborg, P.; Lowe, V. M.; Marshall, P.; Fernandes, R.; Shu, B. An experimental and modeling study on auto-ignition kinetics of ammonia/methanol mixtures at intermediate temperature and high pressure. *Combustion and Flame* **2022**, *242*, 112160.

(37) Nadiri, S.; Shu, B.; Goldsmith, C. F.; Fernandes, R. Development of comprehensive kinetic models of ammonia/methanol ignition using Reaction Mechanism Generator (RMG). *Combustion and Flame* **2023**, *251*, 112710.

(38) Reiter, A. J.; Kong, S.-C. Combustion and emissions characteristics of compression-ignition engine using dual ammonia-diesel fuel. *Fuel* **2011**, *90*, 87–97.

(39) Boretti, A. Novel dual fuel diesel-ammonia combustion system in advanced TDI engines. *International Journal of Hydrogen Energy* **2017**, *42*, 7071–7076.

(40) Tay, K. L.; Yang, W.; Chou, S. K.; Zhou, D.; Li, J.; Yu, W.; Zhao, F.; Mohan, B. Effects of Injection Timing and Pilot Fuel on the Combustion of a Kerosene-diesel/Ammonia Dual Fuel Engine: A Numerical Study. *Energy Procedia* **2017**, *105*, 4621–4626, 8th International Conference on Applied Energy, ICAE2016, 8-11 October 2016, Beijing, China.

(41) Feng, Y.; Zhu, J.; Mao, Y.; Raza, M.; Qian, Y.; Yu, L.; Lu, X. Low-temperature auto-ignition characteristics of NH3/diesel binary fuel: Ignition delay time measurement and kinetic analysis. *Fuel* **2020**, *281*, 118761.

(42) Zhang, J.; Ito, T.; Ishii, H.; Ishihara, S.; Fujimori, T. Numerical investigation on ammonia co-firing in a pulverized coal combustion facility: Effect of ammonia co-firing ratio. *Fuel* **2020**, *267*, 117166.

(43) Ishihara, S.; Zhang, J.; Ito, T. Numerical calculation with detailed chemistry of effect of ammonia co-firing on NO emissions in a coal-fired boiler. *Fuel* **2020**, *266*, 116924.

(44) Green, W. H. Moving from postdictive to predictive kinetics in reaction engineering. *AIChE Journal* **2020**, *66*, e17059.

(45) Kaufman, F. Symposium on Current Status of Kinetics of Elementary Gas Reactions: Predictive Power of Theory and Accuracy of Measurement. *The Journal of Physical Chemistry* **1979**, *83*, 1–3.

(46) Golde, M. Frederick Kaufman 1919-1985, A Biographical Memoir. `http://www.nasonline.org/member-directory/deceased-members/53935.html`, 1995.

(47) Lu, T.; Law, C. K. Toward accommodating realistic fuel chemistry in large-scale computations. *Progress in Energy and Combustion Science* **2009**, *35*, 192–215.

(48) T. Faravelli, E. R., F. Manenti *Mathematical Modelling of Gas-Phase Complex Reaction Systems: Pyrolysis and Combustion*, 1st ed.; Elsevier, 2019; Vol. 45.

(49) Miller, J. A.; Sivaramakrishnan, R.; Tao, Y.; Goldsmith, C. F.; Burke, M. P.; Jasper, A. W.; Hansen, N.; Labbe, N. J.; Glarborg, P.; Zádor, J. Combustion chemistry in the twenty-first century: Developing theory-informed chemical kinetics models. *Progress in Energy and Combustion Science* **2021**, *83*, 100886.

(50) Vernuccio, S.; Broadbelt, L. J. Discerning complex reaction networks using automated generators. *AIChE Journal* **2019**, *65*, e16663.

(51) Frenklach, M. Transforming data into knowledge—Process Informatics for combustion chemistry. *Proceedings of the Combustion Institute* **2007**, *31*, 125–140.

(52) Glarborg, P.; Miller, J. A.; Ruscic, B.; Klippenstein, S. J. Modeling nitrogen chemistry in combustion. *Progress in Energy and Combustion Science* **2018**, *67*, 31–68.

(53) Otomo, J.; Koshi, M.; Mitsumori, T.; Iwasaki, H.; Yamada, K. Chemical kinetic modeling of ammonia oxidation with improved reaction mechanism for ammonia/air and ammonia/hydrogen/air combustion. *International Journal of Hydrogen Energy* **2018**, *43*, 3004–3014.

(54) Shrestha, K. P.; Seidel, L.; Zeuch, T.; Mauss, F. Detailed Kinetic Mechanism for the Oxidation of Ammonia Including the Formation and Reduction of Nitrogen Oxides. *Energy & Fuels* **2018**, *32*, 10202–10217.

(55) Mei, B.; Zhang, X.; Ma, S.; Cui, M.; Guo, H.; Cao, Z.; Li, Y. Experimental and kinetic modeling investigation on the laminar flame propagation of ammonia under oxygen enrichment and elevated pressure conditions. *Combustion and Flame* **2019**, *210*, 236–246.

(56) Li, R.; Konnov, A. A.; He, G.; Qin, F.; Zhang, D. Chemical mechanism development and reduction for combustion of NH3/H2/CH4 mixtures. *Fuel* **2019**, *257*, 116059.

(57) Stagni, A.; Cavallotti, C.; Arunthanayothin, S.; Song, Y.; Herbinet, O.; Battin-Leclerc, F.; Faravelli, T. An experimental, theoretical and kinetic-modeling study of the gas-phase oxidation of ammonia. *React. Chem. Eng.* **2020**, *5*, 696–711.

(58) Issayev, G.; Giri, B. R.; Elbaz, A. M.; Shrestha, K. P.; Mauss, F.; Roberts, W. L.; Farooq, A. Combustion behavior of ammonia blended with diethyl ether. *Proceedings of the Combustion Institute* **2021**, *38*, 499–506.

(59) Arunthanayothin, S.; Stagni, A.; Song, Y.; Herbinet, O.; Faravelli, T.; Battin-Leclerc, F. Ammonia–methane interaction in jet-stirred and flow reactors: An experimental and kinetic modeling study. *Proceedings of the Combustion Institute* **2021**, *38*, 345–353.

(60) Bertolino, A.; Fürst, M.; Stagni, A.; Frassoldati, A.; Pelucchi, M.; Cavallotti, C.; Faravelli, T.; Parente, A. An evolutionary, data-driven approach for mechanism optimization: theory and application to ammonia combustion. *Combustion and Flame* **2021**, *229*, 111366.

(61) Zhang, X.; Moosakutty, S. P.; Rajan, R. P.; Younes, M.; Sarathy, S. M. Combustion chemistry of ammonia/hydrogen mixtures: Jet-stirred reactor measurements and comprehensive kinetic modeling. *Combustion and Flame* **2021**, *234*, 111653.

(62) Shrestha, K. P.; Lhuillier, C.; Barbosa, A. A.; Brequigny, P.; Contino, F.; Mounaïm-Rousselle, C.; Seidel, L.; Mauss, F. An experimental and modeling study of ammonia with enriched oxygen content and ammonia/hydrogen laminar flame speed at elevated pressure and temperature. *Proceedings of the Combustion Institute* **2021**, *38*, 2163–2174.

(63) Shrestha, K. P.; Giri, B. R.; Elbaz, A. M.; Issayev, G.; Roberts, W. L.; Seidel, L.; Mauss, F.; Farooq, A. A detailed chemical insights into the kinetics of diethyl ether enhancing ammonia combustion and the importance of NOx recycling mechanism. *Fuel Communications* **2022**, *10*, 100051.

(64) Gotama, G. J.; Hayakawa, A.; Okafor, E. C.; Kanoshima, R.; Hayashi, M.; Kudo, T.; Kobayashi, H. Measurement of the laminar burning velocity and kinetics study of the importance of the hydrogen recovery mechanism of ammonia/hydrogen/air premixed flames. *Combustion and Flame* **2022**, *236*, 111753.

(65) Zhang, J.; Mei, B.; Li, W.; Fang, J.; Zhang, Y.; Cao, C.; Li, Y. Unraveling Pressure Effects in Laminar Flame Propagation of Ammonia: A Comparative Study with Hydrogen, Methane, and Ammonia/Hydrogen. *Energy & Fuels* **2022**, *36*, 8528–8537.

(66) Liu, J.; Zou, C.; Luo, J. Experimental and modeling study on the ignition delay times

of ammonia/methane mixtures at high dilution and high temperatures. *Proceedings of the Combustion Institute* **2022**,

(67) Tang, R.; Xu, Q.; Pan, J.; Gao, J.; Wang, Z.; Wei, H.; Shu, G. An experimental and modeling study of ammonia oxidation in a jet stirred reactor. *Combustion and Flame* **2022**, *240*, 112007.

(68) García-Ruiz, P.; Uruén, M.; Abián, M.; Alzueta, M. High pressure ammonia oxidation in a flow reactor. *Fuel* **2023**, *348*, 128302.

(69) Zhang, X.; Yalamanchi, K. K.; Mani Sarathy, S. Combustion chemistry of ammonia/C1 fuels: A comprehensive kinetic modeling study. *Fuel* **2023**, *341*, 127676.

(70) Singh, A. S.; Mohapatra, S.; Boyapati, R.; Elbaz, A. M.; Dash, S. K.; Roberts, W. L.; Reddy, V. M. Chemical Kinetic Modeling of the Autoignition Properties of Ammonia at Low–Intermediate Temperature and High Pressure using a Newly Proposed Reaction Mechanism. *Energy & Fuels* **2021**, *35*, 13506–13522.

(71) Hamdy, M.; Nadiri, S.; Mohamed, A.; Dong, S.; Wu, Y.; Fernandes, R.; Zhou, C.; Liu, S.; Senecal, K.; Zhang, K. et al. An Updated Comprehensive Chemical Kinetic Mechanism for Ammonia and its Blends with Hydrogen, Methanol, and <italic>N</italic>-Heptane. WCX SAE World Congress Experience. 2023.

(72) Bugler, J.; Somers, K. P.; Simmie, J. M.; Güthe, F.; Curran, H. J. "Modeling Nitrogen Species as Pollutants: Thermochemical Influences". *The Journal of Physical Chemistry A* **2016**, *120*, 7192–7197.

(73) Klippenstein, S. J.; Glarborg, P. Theoretical kinetics predictions for NH2+HO2. *Combustion and Flame* **2022**, *236*, 111787.

(74) Bugler, J.; Somers, K. P.; Silke, E. J.; Curran, H. J. Revisiting the Kinetics and Thermodynamics of the Low-Temperature Oxidation Pathways of Alkanes: A Case

Study of the Three Pentane Isomers. *The Journal of Physical Chemistry A* **2015**, *119*, 7510–7527.

(75) Kawka, L.; Juhász, G.; Papp, M.; Nagy, T.; Zsély, I. G.; Turányi, T. Comparison of detailed reaction mechanisms for homogeneous ammonia combustion. *Zeitschrift für Physikalische Chemie* **2020**, *234*, 1329–1357.

(76) Valera-Medina, A.; Amer-Hatem, F.; Azad, A. K.; Dedoussi, I. C.; de Joannon, M.; Fernandes, R. X.; Glarborg, P.; Hashemi, H.; He, X.; Mashruk, S. et al. Review on Ammonia as a Potential Fuel: From Synthesis to Economics. *Energy & Fuels* **2021**, *35*, 6964–7029.

(77) Simmie, J. M. Detailed chemical kinetic models for the combustion of hydrocarbon fuels. *Progress in Energy and Combustion Science* **2003**, *29*, 599–634.

(78) Wang, H.; Sheen, D. A. Combustion kinetic model uncertainty quantification, propagation and minimization. *Progress in Energy and Combustion Science* **2015**, *47*, 1–31.

(79) Liu, M.; Dana, A. G.; Johnson, M.; Goldman, M.; Jocher, A.; Payne, A.; Han, C. G. K.; Yee, N.; Mazeau, E.; Blondal, K. et al. Reaction Mechanism Generator v3.0: Advances in Automatic Mechanism Generation. *Journal of Chemical Information and Modeling* **2021**, *61*, 2686–2696.

(80) Johnson, M. S.; Dong, X.; Grinberg Dana, A.; Chung, Y.; Farina, D.; Gillis, R. J.; Liu, M.; Yee, N. W.; Blondal, K.; Mazeau, E. et al. The RMG Database for Chemical Property Prediction. *Chemical Information* **2022**, *62*, 4906–4915.

(81) Gao, C. W.; Allen, J. W.; Green, W. H.; West, R. H. Reaction Mechanism Generator: Automatic construction of chemical kinetic mechanisms. *Computer Physics Communications* **2016**, *203*, 212–225.

(82) Green, W. H. Moving from postdictive to predictive kinetics in reaction engineering. *AIChE Journal* **2020**, *66*, e17059.

(83) Dana, A. G.; Buesser, B.; Merchant, S. S.; Green, W. H. Automated Reaction Mechanism Generation Including Nitrogen as a Heteroatom. *International Journal of Chemical Kinetics* **2018**, *50*, 243–258.

(84) Grinberg Dana, A.; Liu, M.; Green, W. H. Automated chemical resonance generation and structure filtration for kinetic modeling. *International Journal of Chemical Kinetics* **2019**, *51*, 760–776.

(85) Burke, M. P.; Chaos, M.; Ju, Y.; Dryer, F. L.; Klippenstein, S. J. Comprehensive H2/O2 kinetic model for high-pressure combustion. *International Journal of Chemical Kinetics* **2012**, *44*, 444–474.

(86) Konnov, A. A. On the role of excited species in hydrogen combustion. *Combustion and Flame* **2015**, *162*, 3755–3772.

(87) Konnov, A. A. Yet another kinetic mechanism for hydrogen combustion. *Combustion and Flame* **2019**, *203*, 14–22.

(88) Burke, M. P.; Klippenstein, S. J. Ephemeral collision complexes mediate chemically termolecular transformations that affect system chemistry. *Nature Chemistry* **2017**, *9*, 1078–1082.

(89) Grinberg Dana, A.; Moore, K. B. I.; Jasper, A. W.; Green, W. H. Large Intermediates in Hydrazine Decomposition: A Theoretical Study of the N3H5 and N4H6 Potential Energy Surfaces. *The Journal of Physical Chemistry A* **2019**, *123*, 4679–4692.

(90) Dana, A. G. The RMG Primary Nitrogen Kinetics Library. `https://github.com/ReactionMechanismGenerator/RMG-database/blob/main/input/kinetics/libraries/primaryNitrogenLibrary/reactions.py`.

(91) Venkatesh, P. K.; Carr, R. W.; Cohen, M. H.; Dean, A. M. Microcanonical Transition State Theory Rate Coefficients from Thermal Rate Constants via Inverse Laplace Transformation. *J. Phys. Chem. A* **1998**, *102*, 8104–8115.

(92) Dana, A. G.; Johnson, M. S.; Allen, J. W.; Sharma, S.; Raman, S.; Liu, M.; Gao, C. W.; Grambow, C. A.; Goldman, M. J.; Ranasinghe, D. S. et al. Automated reaction kinetics and network exploration (Arkane): A statistical mechanics, thermodynamics, transition state theory, and master equation software. *International Journal of Chemical Kinetics* **2023**, *55*, 300–323.

(93) Chang, A.; Bozzelli, J.; Dean, A. Kinetic Analysis of Complex Chemical Activation and Unimolecular Dissociation Reactions using QRRK Theory and the Modified Strong Collision Approximation. *Zeitschrift für Physikalische Chemie* **2000**, *214*, 1533.

(94) Song, J.; Stephanopoulos, G.; Green, W. H. Valid parameter range analyses for chemical reaction kinetic models. *Chemical Engineering Science* **2002**, *57*, 4475–4491.

(95) Goodwin, D. G.; Moffat, H. K.; Schoegl, I.; Speth, R. L.; Weber, B. W. Cantera: An Object-oriented Software Toolkit for Chemical Kinetics, Thermodynamics, and Transport Processes. `https://www.cantera.org`, 2022; Version 2.6.0.

(96) CHEMKIN-PRO 15112, Reaction Design: San Diego, 2011.

(97) Grinberg Dana, A.; Ranasinghe, D.; Wu, H.; Grambow, C.; Dong, X.; Johnson, M.; Goldman, M.; Liu, M.; Green, W. ARC - Automated Rate Calculator, version 1.1.0. `https://github.com/ReactionMechanismGenerator/ARC`, 2019.

(98) Halgren, T. A. MMFF VI. MMFF94s option for energy minimization studies. *Journal of Computational Chemistry* **1999**, *20*, 720–729.

(99) Landrum, G. RDKit: Open-Source Cheminformatics Software. `http://www.rdkit.org`, `http://www.rdkit.org`.

(100) Grimme, S. Semiempirical hybrid density functional with perturbative second-order correlation. *The Journal of Chemical Physics* **2006**, *124*, 034108.

(101) Grimme, S.; Antony, J.; Ehrlich, S.; Krieg, H. A consistent and accurate ab initio parametrization of density functional dispersion correction (DFT-D) for the 94 elements H-Pu. *The Journal of Chemical Physics* **2010**, *132*, 154104.

(102) Dunning, J., Thom H. Gaussian basis sets for use in correlated molecular calculations. I. The atoms boron through neon and hydrogen. *The Journal of Chemical Physics* **1989**, *90*, 1007–1023.

(103) Alecu, I. M.; Zheng, J.; Zhao, Y.; Truhlar, D. G. Computational Thermochemistry: Scale Factor Databases and Scale Factors for Vibrational Frequencies Obtained from Electronic Model Chemistries. *Journal of Chemical Theory and Computation* **2010**, *6*, 2872–2887.

(104) Adler, T. B.; Knizia, G.; Werner, H.-J. A simple and efficient CCSD(T)-F12 approximation. *The Journal of Chemical Physics* **2007**, *127*, 221106.

(105) Peterson, K. A.; Adler, T. B.; Werner, H.-J. Systematically convergent basis sets for explicitly correlated wavefunctions: The atoms H, He, B–Ne, and Al–Ar. *The Journal of Chemical Physics* **2008**, *128*, 084102.

(106) Werner, H.-J.; Knowles, P. J.; Knizia, G.; Manby, F. R.; Schütz, M. Molpro: a general-purpose quantum chemistry program package. *WIREs Computational Molecular Science* **2012**, *2*, 242–253.

(107) Petersson, G. A.; Malick, D. K.; Wilson, W. G.; Ochterski, J. W.; Montgomery, J., J. A.; Frisch, M. J. Calibration and comparison of the Gaussian-2, complete basis set, and density functional methods for computational thermochemistry. *The Journal of Chemical Physics* **1998**, *109*, 10570–10579.

(108) Ruscic, B. Active Thermochemical Tables (ATcT) values based on ver. 1.124 of the Thermochemical Network, 2023. `http://atct.anl.gov/`.

(109) Frisch, M. J.; Trucks, G. W.; Schlegel, H. B.; Scuseria, G. E.; Robb, M. A.; Cheeseman, J. R.; Scalmani, G.; Barone, V.; Mennucci, B.; Petersson, G. A. et al. Gaussian 09, Revision D.01. Gaussian, Inc., Wallingford CT, 2013.

(110) Montgomery, J., J. A.; Frisch, M. J.; Ochterski, J. W.; Petersson, G. A. A complete basis set model chemistry. VII. Use of the minimum population localization method. *The Journal of Chemical Physics* **2000**, *112*, 6532–6542.

(111) Chai, J.-D.; Head-Gordon, M. Long-range corrected hybrid density functionals with damped atom–atom dispersion corrections. *Phys. Chem. Chem. Phys.* **2008**, *10*, 6615–6620.

(112) Mitnik, N.; Haba, S.; Grinberg Dana, A. Non-physical Species in Chemical Kinetic Models: A Case Study of Diazenyl Hydroxy and Diazenyl Peroxide**. *ChemPhysChem* **2022**, *23*, e202200373.

(113) Cavallotti, C.; Pelucchi, M.; Georgievskii, Y.; Klippenstein, S. J. EStokTP: Electronic Structure to Temperature- and Pressure-Dependent Rate Constants—A Code for Automatically Predicting the Thermal Kinetics of Reactions. *Journal of Chemical Theory and Computation* **2019**, *15*, 1122–1145.

(114) Schlegel, H. B. Optimization of equilibrium geometries and transition structures. *Journal of Computational Chemistry* **1982**, *3*, 214–218.

(115) Weigend, F.; Ahlrichs, R. Balanced basis sets of split valence, triple zeta valence and quadruple zeta valence quality for H to Rn: Design and assessment of accuracy. *Phys. Chem. Chem. Phys.* **2005**, *7*, 3297–3305.

(116) Ishida, K.; Morokuma, K.; Komornicki, A. The intrinsic reaction coordinate. An ab initio calculation for HNC -> HCN and H- + CH4 -> CH4 + H-. *The Journal of Chemical Physics* **2008**, *66*, 2153–2156.

(117) Konnov, A. A. An exploratory modelling study of chemiluminescence in ammonia-fuelled flames. Part 2. *Combustion and Flame* **2023**, 112789.

(118) RMG-Py "thermo_DFT_CCSDTF12_BAC" thermodynamic library in the RMG database. Accessed: April 2023; `https://github.com/ReactionMechanismGenerator/RMG-database/blob/main/input/thermo/libraries/thermo_DFT_CCSDTF12_BAC.py`.

(119) Rasmussen, C. L.; Hansen, J.; Marshall, P.; Glarborg, P. Experimental measurements and kinetic modeling of CO/H2/O2/NOx conversion at high pressure. *International Journal of Chemical Kinetics* **2008**, *40*, 454–480.

(120) Coppens, F.; De Ruyck, J.; Konnov, A. The effects of composition on burning velocity and nitric oxide formation in laminar premixed flames of CH4 + H2 + O2 + N2. *Combustion and Flame* **2007**, *149*, 409–417.

(121) GRI-Mech 3.0, http://combustion.berkeley.edu/gri-mech/.

(122) Sarkisov, O. M.; Cheskis, S. G.; Nadtochenko, V. A.; Sviridenkov, E. A.; Vedeneev, V. I. Spectroscopic study of elementary reactions involving HCO, NH2 and HNO. *Arch. Combust.* **1984**, *4*, 111–120.

(123) Dean, A. M.; Bozzelli, J. W. Combustion Chemistry of Nitrogen. In *Gas-Phase Combustion Chemistry*; Gardiner, W. C., Ed.; Springer New York: New York, NY, 2000; pp 125–341.

(124) Sumathi, R.; Peyerimhoff, S. A quantum statistical analysis of the rate constant for the HO2 + NH2 reaction. *Chemical Physics Letters* **1996**, *263*, 742–748.

(125) Chavarrio Cañas, J. E.; Monge-Palacios, M.; Zhang, X.; Sarathy, S. M. Probing the gas-phase oxidation of ammonia: Addressing uncertainties with theoretical calculations. *Combustion and Flame* **2022**, *235*, 111708.

(126) Miller, J. A.; Glarborg, P. Modelling the Formation of N2O and NO2 in the Thermal De-NOx Process. In *Gas Phase Chemical Reaction Systems*; Wolfrum, J., Volpp, H.-R., Rannacher, R., Warnatz, J., Eds.; Springer Berlin Heidelberg: Berlin, Heidelberg, 1996; pp 318–333.

(127) Klippenstein, S. J.; Harding, L. B.; Glarborg, P.; Miller, J. A. The role of NNH in NO formation and control. *Combustion and Flame* **2011**, *158*, 774–789, Special Issue on Kinetics.

(128) Tsang, W.; Herron, J. T. Chemical Kinetic Data Base for Propellant Combustion I. Reactions Involving NO, NO2, HNO, HNO2, HCN and N2O. *Journal of Physical and Chemical Reference Data* **1991**, *20*, 609–663.

(129) Chen, X.; Fuller, M. E.; Franklin Goldsmith, C. Decomposition kinetics for HONO and HNO2. *React. Chem. Eng.* **2019**, *4*, 323–333.

(130) Miller, J. A.; Bowman, C. T. Mechanism and modeling of nitrogen chemistry in combustion. *Progress in Energy and Combustion Science* **1989**, *15*, 287–338.

(131) Stothard, N.; Humpfer, R.; Grotheer, H.-H. The multichannel reaction NH2 + NH2 at ambient temperature and low pressures. *Chemical Physics Letters* **1995**, *240*, 474–480.

(132) Klippenstein, S. J.; Harding, L. B.; Ruscic, B.; Sivaramakrishnan, R.; Srinivasan, N. K.; Su, M.-C.; Michael, J. V. Thermal Decomposition of NH2OH and Subsequent Reactions: Ab Initio Transition State Theory and Reflected Shock Tube Experiments. *The Journal of Physical Chemistry A* **2009**, *113*, 10241–10259.

(133) Konnov, A. Implementation of the NCN pathway of prompt-NO formation in the detailed reaction mechanism. *Combustion and Flame* **2009**, *156*, 2093–2105.

(134) Zheng, J.; Rocha, R. J.; Pelegrini, M.; Ferrão, L. F. A.; Carvalho, E. F. V.; Roberto-Neto, O.; Machado, F. B. C.; Truhlar, D. G. A product branching ratio controlled by vibrational adiabaticity and variational effects: Kinetics of the H + trans-N2H2 reactions. *The Journal of Chemical Physics* **2012**, *136*, 184310.

(135) Diévart, P.; Catoire, L. Contributions of Experimental Data Obtained in Concentrated Mixtures to Kinetic Studies: Application to Monomethylhydrazine Pyrolysis. *The Journal of Physical Chemistry A* **2020**, *124*, 6214–6236.

(136) Detailed Reaction Mechanism for Small Hydrocarbons Combustion. 2000; `http://homepages.vub.ac.be/~akonnov/`.

(137) Chakraborty, D.; Park, J.; Lin, M. Theoretical study of the OH+NO2 reaction: formation of nitric acid and the hydroperoxyl radical. *Chemical Physics* **1998**, *231*, 39–49.

(138) Zhu, R. S.; Lin, M. C. Ab initio study of the HO2+NO reaction: Prediction of the total rate constant and product branching ratios for the forward and reverse processes. *The Journal of Chemical Physics* **2003**, *119*, 10667–10677.

(139) McBride, B.; Zehe, M.; Gordon, S. NASA Glenn Coefficients for Calculating Thermodynamic Properties of Individual Species. `https://ntrs.nasa.gov/api/citations/20020085330/downloads/20020085330.pdf`, 2002; `https://ntrs.nasa.gov/api/citations/20020085330/downloads/20020085330.pdf`.

(140) RMG-Py "NH3" thermodynamic library in the RMG database. Accessed: August 2023; `https://github.com/ReactionMechanismGenerator/RMG-database/blob/nh3/input/thermo/libraries/NH3.py`.

(141) Weininger, D. SMILES, a Chemical Language and Information System. 1. Introduction to Methodology and Encoding Rules. *J. Chem. Inf. Comput. Sci.* **1988**, *28*, 31–36.

(142) Stagni, A.; Cavallotti, C.; Arunthanayothin, S.; Song, Y.; Herbinet, O.; Battin-Leclerc, F.; Faravelli, T. An experimental, theoretical and kinetic-modeling study of the gas-phase oxidation of ammonia. *React. Chem. Eng.* **2020**, *5*, 696–711.

(143) Hanson, R. K.; Salimian, S. Survey of Rate Constants in the N/H/O System. In *Combustion Chemistry*; Gardiner, W. C., Ed.; Springer New York: New York, NY, 1984; pp 361–421.

(144) Baev, V. M.; Sarkisov, I. N.; Sviridenkov, E. A.; Suchkov, A. F. Intracavity laser spectroscopy. *Journal of Soviet Laser Research* **1989**, *10*, 61–85.

(145) Glarborg, P.; Dam-Johansen, K.; Miller, J. A.; Kee, R. J.; Coltrin, M. E. Modeling the thermal DENOx process in flow reactors. Surface effects and Nitrous Oxide formation. *International Journal of Chemical Kinetics* **1994**, *26*, 421–436.